HHS Public Access

Author manuscript

Pain. Author manuscript; available in PMC 2024 December 01.

Published in final edited form as:

Pain. 2023 December 01; 164(12): 2696–2710. doi:10.1097/j.pain.0000000000002970.

Neuropilin-1 is essential for VEGFA-mediated increase of sensory neuron activity and development of pain-like behaviors

Kimberly Gomez[1,2,‡], **Paz Duran**[1,2,‡], **Raquel Tonello**[1,2], **Heather N. Allen**[1,2], **Lisa Boinon**[3], **Aida Calderon-Rivera**[1,2], **Santiago Loya-López**[1,2], **Tyler S. Nelson**[1,2], **Dongzhi Ran**[3], **Aubin Moutal**[4], **Nigel W. Bunnett**[1,2,5], **Rajesh Khanna**[1,2,5,*]

[1]Department of Molecular Pathobiology, College of Dentistry, New York University; New York, NY, United States of America.

[2]NYU Pain Research Center, 433 First Avenue; New York, NY, United States of America.

[3]Department of Pharmacology, College of Medicine, The University of Arizona; Tucson, AZ, United States of America.

[4]School of Medicine, Department of Pharmacology and Physiology, Saint Louis University; Saint Louis, MO, United States of America.

[5]Department of Neuroscience & Physiology, New York University Grossman School of Medicine, New York, NY 10016 USA

1. Introduction

Neuropilins (NRP-1 and NRP-2) are non-tyrosine kinase transmembrane glycoproteins that act as co-receptors for the vascular endothelial growth factor (VEGF) family of proangiogenic cytokines and the class III semaphorin (Sema3) family of axon guidance molecules [53]. NRPs form a complex with other tyrosine kinase receptors: plexin A1 and A2 (PlexA 1–2) (ligand semaphorins [64]) and VEGFR1 and VEGFR2 (receptors for VEGFB and VEGFA, respectively [41]) to transduce functional responses involved in neuronal development, immunity, axonal guidance, vascularization, and angiogenesis [11; 21; 53]. Further, NRPs and their receptor complex are implicated in pathological conditions such as cancer [31], human T-cell lymphotropic virus type 1 [20], and severe acute respiratory syndrome coronavirus 2 (SARS-CoV-2) infection [8; 12]. NRP-1 facilitates SARS-CoV-2 entry and infectivity. Notably, a truncated Spike protein bound surface NRP1 and blocking this interaction with a small-molecule inhibitor or monoclonal antibodies reduced viral infection in cell culture [8; 12].

*To whom correspondence should be addressed: Dr. Rajesh Khanna, Department of Molecular Pathobiology, College of Dentistry, New York University, 433 1st Avenue Room 720 New York City, NY 10010, rk4272@nyu.edu.

‡Contributed equally

Author Contributions

R.K. developed the concept, designed the experiments, and supervised all aspects of this project. R.K., A.M., and N.W.B. designed and supervised experiments and advised in data analysis. K.G., P.D., and R.K. wrote the manuscript. K.G., D.R., L.B., A.C.-R. and S.L. performed electrophysiological recordings. A.M. designed the CRISPR editing gRNAs. P.D. performed biochemistry experiments and prepared the figures. R.T. and K.G. performed the behavioral experiments. H.N.A and T.S.N. performed RNAscope® fluorescence *in situ* hybridization and helped with writing of the manuscript. K.G. and R.T. performed behavioral experiments. All authors had the opportunity to discuss the results and comment on the manuscript.

VEGFA, a major ligand of NRP-1 receptors, enhances pain behaviors in normal, nerve-injured, and diabetic animals [27; 60; 69]. Clinical findings support that VEGFA potently contributes to pain manifestation; for example, increased VEGFA expression is associated with higher pain scores in osteoarthritis [65], complex regional pain syndrome [50], endometriosis [49], and back pain [42]. Previously, we found that VEGFA increased voltage-gated sodium and calcium channel activity in dorsal root ganglion (DRG) sensory neurons and enhanced synaptic activity in the spinal dorsal horn (SDH) [44]. Further, we found that both the SARS-CoV-2 Spike protein and EG00229 (a small molecule NRP-1 inhibitor [29]): (*i*) blocked VEGFA-induced mechanical allodynia and thermal hyperalgesia in naïve rats [45], (*ii*) reversed mechanical allodynia in the spared nerve injury model of neuropathic pain, and (*iii*) blocked VEGFA-induced nociceptor sensitization [45]. This effect was mediated by a VEGFA-induced increase of voltage-gated sodium and calcium channel activity in dorsal root ganglion (DRG) sensory neurons that lead to enhanced synaptic activity in the spinal dorsal horn (SDH) [45].

Other than our reports linking VEGFA/NRP-1 to nociception [45], NRP-1 has not been studied in the context of pain. Furthermore, as NRP-1 is upregulated in rat and human DRG neurons after a traumatic nerve injury [38], it is important to validate NRP-1 as a pain target prior to embarking on drug discovery campaigns. Therefore, here we used biochemical, genetic, electrophysiological, and behavioral approaches to test the functional role of NRP-1 in sensory neurons and VEGFA-induced pain. We hypothesized that NRP-1 deletion in DRG and SDH neurons would reduce VEGFA's pro-nociceptive actions. We found that NRP-1 is expressed in putative nociceptors and that clustered regularly interspaced short palindromic repeats and CRISPR-associated protein 9 (CRISPR/Cas9) editing of NRP-1 in sensory neurons prevented a VEGFA-mediated increase of N-type voltage-gated calcium (CaV2.2), ProTx-II-sensitive (NaV1.7) voltage-gated sodium currents, and spinal cord neurotransmission. Intrathecal injection of a lentivirus packaged with a guide RNA (gRNA) against NRP-1 prevented development of spinal nerve ligation-induced pain behaviors in male and female rats. Our results extend the role of VEGFA in facilitating nociceptive neurotransmission and highlight NRP-1 as a new target for interfering with VEGFA-mediated nociception.

2. Methods

2.1 Animals

All experiments and procedures were performed in accordance with the guidelines recommended by the National Institutes of Health, the International Association for the Study of Pain, and the National Centre for the Replacement, Refinement, and Reduction of Animals in Research (NC3Rs) guidelines. Pathogen-free, adult female Sprague-Dawley rats (100–150 g; Envigo, Placentia, CA) were used for RNAscope® fluorescence *in situ* hybridization, western blot, and electrophysiological recordings of DRG neurons. Pathogen-free, adult male and female Sprague-Dawley rats (100–150 g; Envigo, Placentia, CA) were used for behavioral experiments. Pathogen-free, male Sprague-Dawley rat pups (postnatal 10–15 days; Envigo, Placentia, CA) were used for electrophysiological experiments in spinal cord slices. Animals were housed in the University of Arizona Laboratory Animal

Research Center or New York University Kriser Dental Center Animal Facility in light (12-h light: 12-h dark cycle; lights on at 07:00 h) and temperature (23 ± 3°C) controlled rooms, with standard rodent chow and water *ad libitum*. The Institutional Animal Care and Use Committees of the College of Medicine at the University of Arizona and New York University approved all experiments.

2.2 Reagents

All chemicals, unless noted, were purchased from Sigma (St Louis, MO). Rat VEGFA (Cat# 89–967-005, Fisher Scientific, Hampton, NH) was resuspended in PBS to a stock concentration of 1 μM.

2.3 gRNA strategy for Neuropilin 1 receptor gene targeting

Our strategy to delete Neuropilin 1 in rodents focused on targeting the second exon (ENSRNOT00000080465.1, gRNA: gCTATAAAAATTGAAAACCCG, on-score 73.6, off-score 59.3) on the *Nrp1* gene using a guide RNA (gRNA) as described previously [43; 46; 47]. The target exon was selected to ensure total removal of one of the receptors while ensuring minimal to no off-target activity of the Cas9 enzyme as we and others reported before [39; 47]. The gRNA sequence is based on the rat *Nrp1* gene. The indicated gRNA sequence was inserted into the *Esp3I* restriction site of the pL-CRISPR.EFS.GFP lentiplasmid (Cat# 57819, Addgene, Cambridge, MA) [25]; a plasmid that allows for simultaneous expression of the Cas9 enzyme and the gRNA. The control plasmid consisted of a non-targeting gRNA (gGAGACGTGACCGTCTCT), GFP, and the Cas9 enzyme. All plasmids were verified by Sanger sequencing (Eurofins, Louisville, KY).

2.4 Recombinant lentivirus production

Lentivirus particles containing pL-CRISPR-EFS-GFP-NRP-1 or pL-CRISPR-EFS-GFP (as control) were packaged as described previously [6]. Briefly, HEK293T cells were transfected with the plasmid vector system and the packaging plasmids to provide the VSV-G envelope. Two days post-transfection, the virus-containing medium was collected, and debris was removed by centrifugation. Virus was concentrated by ultracentrifugation, and the viral pellet was suspended in Dulbecco's modified Eagle's medium supplemented with 10% fetal bovine serum, passed through a 0.45-μm filter, and frozen at −80 °C. The viral titer, as determined by analysis of the virus-associated p24 core protein (QuickTiter lentivirus quantification kit (Cell Biolabs, Inc., San Diego, CA)), was above 1×10^8 transducing units/ml for all viruses used in this study. Virus particles were produced in the University of Arizona Viral Production Core Facility.

2.5 Preparation of dissociated rat dorsal root ganglion neurons

Dorsal root ganglia from all levels were dissociated as described previously [45] [17]. Female Sprague-Dawley rats (100–150 g) were euthanized according to institutionally approved procedures. Briefly, lumbar DRGs were collected, trimmed at their roots, and enzymatically digested in DMEM (Cat# 11965, Thermo Fisher Scientific, Waltham, MA) media with neutral protease (3.125 mg/mL, Cat# LS02104, Worthington, Lakewood, NJ) and collagenase type I (5 mg/mL, Cat# LS004194, Worthington, Lakewood, NJ) for 50

min at 37 ^{O}C under gentle agitation. The dissociated DRG neurons were gently centrifuged to collect cells and resuspended in complete DRG media (DMEM containing 1% penicillin/streptomycin sulfate from 10,000 μg/mL stock, 30 ng/mL of nerve growth factor, and 10% fetal bovine serum (Hyclone)). Cells were seeded on poly-D-lysine-coated 12 mm coverslips or cell culture dishes.

2.6 Immunoblot preparation and analysis

Indicated samples were loaded on 4–20% Novex gels (Cat# XP04205BOX; Thermo Fisher Scientific, Waltham, MA). Proteins were transferred for 1 h at 100 V using TGS [25 mM Tris, pH 8.5, 192 mM glycine, 0.1% (mass/vol) SDS], 20% (vol/vol) methanol as transfer buffer to polyvinylidene difluoride (PVDF) membranes (0.45 μm; Cat# IPFL00010; Millipore Sigma, St. Louis, MO), preactivated in pure methanol. After transfer, the membranes were blocked at room temperature for 1 h with TBST (50 mM Tris·HCl, pH 7.4, 150 mM NaCl, 0.1% Tween 20) with 5% (mass/vol) nonfat dry milk, and then incubated separately in indicated primary antibodies NRP-1 (Cat# MA5–35253; Research Resource Identifiers (RRIDs):AB_2849156; Thermo Fisher Scientific, Waltham, MA), βIII-Tubulin (Cat# G7121; RRID:AB_430874; Promega, Madison, WI), in TBST, 5% (mass/vol) BSA, overnight at 4 °C. Following incubation in HRP-conjugated secondary antibodies from Jackson Immuno Research (West Grove, PA) (1/10,000 dilution), Mouse Anti-Rabbit (Cat# 211–032-171, RRID:AB_2339149) and Goat Anti-Mouse (Cat# 115–035-174, RRID:AB_2338512), blots were revealed by enhanced luminescence (Cat# WBKLS0500; Millipore Sigma, St. Louis, MO) before exposure to photographic film as described [33].

2.7 Electrophysiological recordings from rat DRG neurons

All recordings were done using procedures adapted from our prior work [45; 54; 72]. Recordings were performed from acutely dissociated DRG neurons from Sprague Dawley rats with a capacitance value below 30 pF, which has been historically associated with the population of small diameter DRG neurons [4]. DRG neurons were incubated for 30 min with either 0.1% PBS or VEGFA (1 nM) and both were added in the recording solution.

For total sodium current recordings, the internal pipette solution consisted of (in mM): 140 CsF, 10 NaCl, 1.1 Cs-EGTA, and 15 HEPES (pH 7.3, mOsm/L = 290–310) and external solution contained (in mM): 140 NaCl, 30 tetraethylammonium chloride, 10 D-glucose, 3 KCl, 1 $CaCl_2$, 0.5 $CdCl_2$, 1 $MgCl_2$, and 10 HEPES (pH 7.3, mOsm/L = 310–315). DRG neurons were interrogated with current-voltage (I-V) and activation/inactivation voltage protocols. The voltage protocols were as follows: (a) I-V protocol: from a holding potential of −60 mV, cells were depolarized with 150-millisecond voltage steps over a range of −70 to +60 mV in +5 - mV increments; (b) inactivation protocol: from a holding potential of −60 mV, cells were subjected to hyperpolarizing/repolarizing pulses for 1 second over a range of −120 to 0 mV in +10 mV steps. This protocol allowed subtraction of electrically isolated tetrodotoxin-resistant (TTX-R; current available after −40 mV prepulse) from total current (current available after −120 mV prepulse). When NaV1.7-blocker was employed, ProTx-II was added into the external recording solution at a final concentration of 5 nM.

For recordings of N-type (CaV2.2) voltage-gated calcium currents the intracellular pipette solution was composed of (in mM): 150 $CsCl_2$, 10 HEPES, 5 Mg-ATP, and 5 BAPTA (pH 7.3, mOsm/L=290–310) and the external solution contained (in mM): 110 NMDG, 10 $BaCl_2$, 30 TEA-Cl, 10 HEPES and 10 glucose (pH 7.3, mOsm/L = ~ 310). To isolate N-type specific calcium currents, the following blockers were used: SNX-482 (200 nM, R-type Ca^{2+} channel blocker), TTA-P2 (1 μM, T-type Ca^{2+} channel blocker), ω-agatoxin (200 nM, P/Q-type Ca^{2+} channel blocker), and nifedipine (10 μM, L-type Ca^{2+} channel blocker). Activation of Ca^{2+} current was measured from a holding voltage of −60 mV for 5 ms followed by 200-ms depolarizing voltage steps from −70 mV to +60 mV in 10-mV increments. Steady-state inactivation of Ca^{2+} current was determined by applying a 1500 ms conditioning prepulse (−100 to +30 mV in +10 mV increments) after which, the voltage was stepped to +10 mV for 200-ms. There were 15-s intervals separating each acquisition to allow channels to revert to their basal state.

To isolate potassium currents, the extracellular solution contained (in mM): 140 N-methyl-glucamine chloride, 5 KCl, 2 $CaCl_2$, 1 $MgCl_2$, 10 HEPES, and 10 glucose, pH adjusted to 7.4 with KOH. Recording pipettes were filled with the following solutions (in mM): 140 KCl, 5 $MgCl_2$, 4 ATP, 0.3 GTP, 2.5 $CaCl_2$, 5 EGTA, and 10 HEPES, adjusted pH at 7.3 with KOH. The membrane was held at −60 mV. The fast-inactivating IK_A was isolated by subtraction of the currents obtained for a conditioning prepulse to −40 mV from those obtained for a prepulse to −100 mV. Initially, a 4-s prepulse to −100 mV was applied followed by voltage steps of 500 milliseconds that ranged from −80 to +40 mV in +20-mV increments at 15-s intervals. This was followed by an identical voltage protocol using a prepulse to −40 mV. IK_A was obtained by digital subtraction of these current traces.

Normalization of currents to each cell's capacitance (pF) was performed to allow for collection of current density data. For I-V curves, functions were fitted to data using a non-linear least squares analysis. I-V curves were fitted using double Boltzmann functions:

$$f = a + g1/(1 + exp((x - V_{1/2}1)/k1)) + g2/(1 + exp(-(x - V_{1/2}2)/k2))$$

where x is the pre-pulse potential, $V_{1/2}$is the mid-point potential and k is the corresponding slope factor for single Boltzmann functions. Double Boltzmann fits were used to describe the shape of the curve, not to imply the existence of separate channel populations. Numbers *1* and *2* simply indicate first and second mid-points; a along with g are fitting parameters.

2.8 Intrathecal injections of plasmids for electrophysiology

Young (P10–13) rats were deeply anesthetized with isoflurane (4% for induction and 2% for maintaining). The lower half of the animal's back was shaved. A 25G needle was introduced, perpendicular to the surface through the widest L4-L5 intervertebral level and lowered until it met the vertebral body. Occasionally, a quick flicking of the tail could be observed and served as a proxy for optimal placement of the needle. The moment of penetration into the intrathecal space could be noticed by a change in resistance to the introduction of the needle. Young rats (P10–13) were injected with 10 μL of indicated Plasmid depending on their treatment group (Control CRISPR vs. NRP1 CRISPR). The

electrophysiology experiments were performed two days following the intrathecal injections to allow plasmid-mediated modulation as described [5; 75].

2.9 Preparation of spinal cord slices

Rats were deeply anesthetized with isoflurane (4% for induction and 2% for maintaining). For spinal nerve block, 0.3 mL of 2% lidocaine was injected to both sides of L4 to L5 lumbar vertebrae. Laminectomy was performed from mid-thoracic to low lumbar levels, and the spinal cord was quickly removed to cold modified ACSF oxygenated with 95% O_2 and 5% CO_2. The ACSF for rat dissection contained the following (in mM): 80 NaCl, 2.5 KCl, 1.25 NaH_2PO_4, 0.5 $CaCl_2$.2H2O, 3.5 $MgCl_2.6H_2O$, 25 $NaHCO_3$, 75 Sucrose, 1.3 ascorbate, 3.0 sodium pyruvate with pH at 7.4 and osmolarity at 310 mOsm. Transverse 400 μm-thick slices were obtained by a vibratome (VT1200S; Leica, Nussloch, Germany). Slices were then incubated for 45 mins at 37°C before a 1h incubation at RT in an oxygenated recording solution containing the following (in mM): 125 NaCl, 2.5 KCl, 1.25 NaH_2PO_4, 2 $CaCl_2.2H_2O$, 1 $MgCl_2.6H_2O$, 26 $NaHCO_3$, 25 D-Glucose, 1.3 ascorbate, 3.0 sodium pyruvate with pH at 7.4 and osmolarity at 320 mOsm. The slices were then positioned in a recording chamber and continuously perfused with oxygenated recording solution at a rate of 3 to 4 mL/min before electrophysiological recordings at room temperature (RT) [5; 75].

2.10 Electrophysiological recordings in spinal cord slices by whole-cell patch-clamp

Substantia Gelatinosa neurons (lamina I/IIa) were visualized and identified in the slices by means of infrared differential interferences contrast video microscopy on an upright microscope (FN1; Nikon, Tokyo, Japan) equipped with a 3.40/0.80 water-immersion objective and a charged-coupled device camera. Patch pipettes with resistance at 6 to 10 MΩ were made from borosilicate glass (Sutter Instruments, Novato, CA) on a four-step micropipette puller (P-90; Sutter Instruments, Novato, CA). For spontaneous excitatory postsynaptic current (sEPSC) recordings the pipette solution contained the following (in mM): 120 potassium-gluconate, 20 KCl, 2 $MgCl_2.6H_2O$, 2.0 Na-ATP, 0.5 Na-GTP, 20 HEPES, 0.5 EGTA with pH at 7.4 and osmolarity at 310 mOsm. For all recordings, the membrane potential was held at −60 mV using a PATCHMASTER software in combination with a patch clamp amplifier (EPC10; HEKA Elektronik, Lambrecht, Germany).

The whole-cell configuration was obtained in voltage-clamp mode. To record sEPSCs, bicuculline methiodide (10 μM, Cat# 14343, Sigma Aldrich) and strychnine (2 μM, Cat# S0532, Sigma Aldrich, St Louis, MO) were added to the recording solution to block γ-aminobutyric acid-activated (GABA) and glycine-activated currents. Hyperpolarizing step pulses (5 mV for 50 milliseconds) were periodically delivered to monitor the access resistance (15–25 MΩ), and recordings were discontinued if the access resistance changed by more than 20%. For each neuron, sEPSCs were recorded for a total duration of 2 minutes. Currents were filtered at 3kHz and digitized at 6 kHz. Data were further analyzed by the Mini-Analysis Program (Synatosoft Inc., NJ) to provide spreadsheets for the generation of cumulative probability plots. The frequency and amplitude of the recordings were compared between neurons from animals in control and the indicated groups.

2.11 Intrathecal administration of lentiviruses for behavior

Lentivirus particles (~ $1x10^6$ IFU/mL for rats) containing pL-CRISPR-EFS-GFP-rNRP-1 or pL-CRISPR-EFS-GFP (as control) were injected intrathecally (5 μl) between L4/L5 intervertebral level into isoflurane anesthetized rats (4% for induction and 2% for maintaining). In rats, 14 days after spinal nerve ligation, intrathecal injections of lentiviruses were performed and behavior was measured 5 days after injection.

2.12 Fluorescence in situ hybridization, imaging, and quantification

One week after intrathecal administration of lentiviral particles (control and NRP-1), rats were deeply anesthetized with isoflurane and euthanized via decapitation. Lumbar (L4 and L5) dorsal root ganglia (DRG) were rapidly extracted via blunt dissection and frozen in optimal cutting temperature (OCT) on dry ice. Tissues were stored at −80 °C until cryosectioning. 18 μm thick sections of DRG tissue were obtained on a cryostat, direct mounted on Superfrost Plus Microscope slides, and air dried overnight at room temperature (RT). The next morning slides underwent pretreatment for RNAscope® fluorescence *in situ* hybridization. First, the slides were dipped into distilled H_2O to remove OCT before a 15-minute bath in 10% neutral buffered formalin (4 °C). Next, the slides were bathed for 5 minutes in 50% ethanol (RT), 5 minutes in 70% ethanol (RT), and then 10 minutes in 100% ethanol (RT). The slides were then dried for 5 minutes (RT), and a hydrophobic barrier was applied around each section using an ImmEdge™ hydrophobic barrier pen. Protease IV was applied to each section for 5 minutes (RT) in the humidity tray (Advanced Cell Diagnostics (ACD), EZ-Batch Slide Holder, Cat # 321716) before beginning the RNAscope® Fluorescent v2 assay (ACD, Cat #: 323110) and hybridization to marker probes. RNAscope® probes used in this study were: Rn-Calca-C3 (ACD, Cat#: 317511-C3), Rn-Nrp1-C1 (ACD, Cat #: 1235601-C1), and Rn-Scn9a-C2 (ACD, Cat#: 317851-C2). The C1 channel (*Nrp1*) was labeled with TSA Vivid Fluorophore 570 (ACD, Cat#: 323272), the C2 channel (*Scn9a*) was labeled with TSA Vivid Fluorophore 520 (ACD, Cat#: 323271), and the C3 channel (*Calca*) was labeled with TSA Vivid Fluorophore 650 (ACD, Cat#: 323273). At the end of the RNAscope® Fluorescent v2 assay the slides were coverslipped with VECTASHIELD® Antifade Mounting Medium with DAPI (Vector Laboratories, Cat#: H-1200–10) and the edges were sealed with nail polish. Stitched images encompassing an entire DRG section were captured on a Leica DMI8 microscope (Wetzlar, Germany) using a 40x objective and analyzed using QuPath software v0.4.3. Cells with at least 15 puncta associated with a DAPI nucleus were considered positive. Each individual dot (Figure 1) represents the mean of 3–8 quantified sections across two DRGs per individual rat. The final images were produced in Adobe Illustrator 2022.

2.13 L5/L6 spinal nerve ligation in rats

Male and female rats (~150 g) were deeply anesthetized with isoflurane (4% for induction and 2% for maintenance). The lower half of the animal's back was shaved. After surgical preparation, the left L5 and L6 spinal nerves were exposed by removing the paraspinal muscles and ligated with a 5–0 silk suture in a region distal to the DRG [26]. After hemostasis was confirmed, muscle and fascia were closed in layers using 5–0 absorbable

suture, and the skin was closed with wound clips. Animals were allowed to recover for 14 days.

2.14 Measurement of mechanical allodynia in rats

Mechanical allodynia was assessed by measuring rats' paw withdrawal threshold in response to probing with a series of fine calibrated filaments (von Frey, Stoelting, Wood Dale, IL). Rats were placed in suspended plastic cages with a wire mesh floor, and each von Frey filament was applied perpendicularly to the plantar surface of the paw. The "up-down" method (sequential increase and decrease of the stimulus strength) was used to determine the withdrawal threshold Dixon's nonparametric method was used for data analysis, as described by Chaplan et al [10]. Data were expressed as the paw withdrawal threshold. Mechanical allodynia was manifested as a decrease in paw withdrawal threshold.

2.15 Measurement of thermal hyperalgesia in rats

To evaluate thermal hyperalgesia, the Hargreaves apparatus was employed (Ugo Basile) [23]. Rats were acclimatized in transparent Plexiglass chambers 1 h before testing. The infrared intensity was set at 50% and cut off time to a maximum of 30 s. Thermal hyperalgesia was manifested as a decrease in paw withdrawal latency. The latency was evaluated before (basal) and at different time points after the treatment.

2.16 Data Analysis

Graphing and statistical analysis was performed with GraphPad Prism (Version 9). All data sets were checked for normality using D'Agostino & Pearson test. Details of statistical tests, significance and sample sizes are reported in the appropriate figure legends and in Table S1. All data plotted represent mean ± SEM. RNAscope® fluorescence *in situ* hybridization analysis was done using Unpaired t test. For western blot experiments statistical differences between groups were determined by Unpaired t tests. For electrophysiological recordings: peak current density was analyzed using One-way ANOVA with Tukey's post hoc test and Kruskal-Wallis test with Dunn's post hoc test. For spinal cord slice recordings, the significance was analyzed by One-way ANOVA with Tukey's post hoc test. $V_{1/2}$ midpoint potential and k slope factor were compared using ANOVA with Tukey's post hoc test. Behavioral data was analyzed by Two-way ANOVA followed by Bonferroni's multiple comparisons test, and area under the curve with Unpaired t-tests.

3. Results

3.1 Neuropilin-1 is expressed in putative nociceptors

First, we used multi-label fluorescence *in situ hybridization* (FISH) to neurochemically characterize *Nrp1* expression in putative nociceptive lumbar (L4-L5) dorsal root ganglia (DRG) neurons from adult female rats (Figure 1A). We found that *Nrp1* is widely distributed in both peptidergic and non-peptidergic sensory neurons as only a subset of *Nrp1*-expressing neurons co-expressed calcitonin gene-related peptide (CGRP) or *Calca* (21.56 ± 4.05%). *Nrp1*-expressing neurons extensively co-expressed the major nociceptive voltage-gated sodium channel marker NaV1.7 or *Scn9a* (69.73 ± 3.68%). Additionally, a primary subset of *Nrp1*-expressing neurons co-expressed both *Calca* and *Scn9a* (19.36 ± 3.29%) (Figure

1B). These results indicate that *Nrp1* is widely distributed in primary sensory neurons with a significant expression in presumptive nociceptors.

3.2 Neuropilin-1 editing using CRISPR/Cas9

To interrogate the functions of NRP-1 in nociceptive signaling, we employed a CRISPR/Cas9 editing strategy targeting the second exon of the gene coding for NRP-1 to selectively delete this receptor. We then constructed a CRISPR/Cas9 lentiviral plasmid for NRP-1 gene editing for *in vivo* validation. Next, control gRNA with Cas9 and NRP-1 gRNA with Cas9 lentiviruses ($1x10^6$ live particles in 5 μL) were intrathecally (i.t.) injected into the lumbar region of the spinal cords of naïve rats. Seven days following injection, DRGs were collected. We found that at the RNA level, rats injected with NRP-1 gRNA with Cas9 lentiviruses showed a successful knockdown of *Nrp1* in the DRGs, which was manifested as a significant decrease in the number of *Nrp1* positive cells (Figure 2A and B).

Next, to corroborate NRP-1 knockdown at the protein level, we performed *in vitro* an *in vivo* validation for our subsequent *in vitro* DRG recordings and *in vivo* behavioral assessments. First, rat DRG neurons were dissociated and isolated as described in Moutal et al. (2021) and then transfected with a control empty gRNA plasmid with Cas9 (pL-CRISPR-EFS-GFP) and a plasmid containing a *nrp-1* targeting gRNA with Cas9 to edit NRP-1 (pL-CRISPR-EFS-GFP-rNRP-1). Two days following transfection, western blot analysis with a validated antibody against NRP-1 was used to test knockdown. A significant decrease in NRP-1 expression levels was observed in the NRP-1 gRNA transfected DRGs compared with empty plasmid-transfected DRGs (pL-CRISPR-EFS-GFP: 1.000 ± 0.061; pL-CRISPR-EFS-GFP-rNRP-1: 0.324 ± 0.087; p=0.0007; Figure 2C and D, and Table S1). Next, from the rats intrathecally injected with control gRNA Cas9 lentivirus and NRP-1 gRNA Cas9 lentivirus ($1x10^6$ live particles in 5 μL), we obtained DRGs and lumbar spinal cords seven days after infection. We then isolated proteins and performed western blot analysis to measure protein levels. We found that in both DRGs and spinal cords, a significant decrement in NRP-1 expression was observed after injecting rats with NRP-1 gRNA Cas9 lentivirus, when compared to rats injected with control gRNA Cas9 lentivirus (DRGs- Control gRNA Cas9 lentivirus: 1.000 ± 0.069; NRP-1 gRNA Cas9 lentivirus: 0.793 ± 0.045; p=0.0226; Figure 2E and F. Spinal cord- Control gRNA Cas9 lentivirus: 1.000 ± 0.059; NRP-1 gRNA Cas9 lentivirus: 0.803 ± 0.071; p=0.0495; Figure 2G and H, and Table S1). Our results show a significant knockdown of the expression of NRP-1 at the RNA and protein levels, thus validating the CRISPR/Cas9 editing approach for the following experiments.

3.3 Knockdown of NRP-1 attenuates VEGFA-induced increase in sodium currents

We previously reported that binding of VEGFA to VEGFR2/NRP-1 triggers intracellular events that increase voltage-gated sodium and calcium channel activity in sensory neurons [45]. Therefore, we first assessed if knocking down NRP-1 in rat DRG neurons could prevent VEGFA-mediated increase in sodium currents (Figure 3). Two days after transfecting control plasmid (pL-CRISPR-EFS-GFP) and NRP-1 gRNA plasmid (pL-CRISPR-EFS-GFP-rNRP-1) into rat sensory neurons, sodium currents were recorded. Typical Na^+ current families from small-to-medium sized DRG neurons elicited by rectangular depolarizing pulses from −70 to +60 mV are shown in Figure 3A. In DRG

neurons transfected with control plasmid, incubation with VEGFA (1 nM) resulted in a significant increase of sodium currents (Figure 3A), current density (Figure 3B), as well as peak sodium current density (pL-CRISPR-EFS-GFP: −142.2 ± 17.0 pA/pF; pL-CRISPR-EFS-GFP + VEGFA: −329.4 ± 67.1 pA/pF; p=0.0424; Figure 3C and Table S1), which correlate with our earlier findings [45]. Knocking-down NRP-1 did not affect Na^+ currents (pL-CRISPR-EFS-GFP: −142.2 ± 17.0 pA/pF; pL-CRISPR-EFS-GFP-rNRP-1: −134.9 ± 22.6 pA/pF; p=0.9244; Figure 3C and Table S1). In contrast, VEGFA mediated increase in sodium current density was normalized in cells with knockdown of NRP-1 (pL-CRISPR-EFS-GFP + VEGFA: −329.4 ± 67.1 pA/pF; pL-CRISPR-EFS-GFP-rNRP-1+ VEGFA: −99.3 ± 8.9 pA/pF; p=0.0051; Figure 3C and Table S1). We also determined whether activation and inactivation kinetics of DRG Na^+ channels were affected. No difference in half-maximal activation and inactivation ($V_{1/2}$), as well as slope values (k) for activation and inactivation were observed between the four groups (Figure 3D and Table S2). Importantly, the current density of tetrodotoxin-resistant (TTX-R) channels - NaV1.8 and NaV1.9 - was not affected in any of these conditions (Figure 3E). These results validate our previous findings that NRP-1 is needed for VEGFA-induced potentiation of sodium currents in nociceptive DRG neurons.

3.4 NaV1.7 sodium channel is a target effector protein of VEGFA/NRP-1 axis

Since NaV1.7 channels are TTX-S channels that play a key role in action potential generation in DRG neurons and are the main contributors to human pain signaling [13; 35], we evaluated whether these channels contributed to VEGFA-induced enhancement of TTX-S sodium currents using the NaV1.7-selective blocker Protoxin-II (ProTx-II) [58]. Two days following transfection of the gRNA/Cas9 plasmids, we recorded sodium currents from DRG neurons in the presence of VEGFA with and without co-treatment with this toxin (Figure 4A). Consistent with the data above, treatment of pL-CRISPR-EFS-GFP transfected neurons with VEGFA enhanced sodium currents (Figure 4A) and current density (Figure 4B and C). Co-treatment of these cells with ProTx-II attenuated VEGFA-mediated increase in sodium current density (pL-CRISPR-EFS-GFP + VEGFA: −371.9 ± 37.1 pA/pF; pL-CRISPR-EFS-GFP + VEGFA + ProTx-II: −209.5 ± 28.9 pA/pF; p=0.0067; Figure 4C and Table S1), to a magnitude like that of pL-CRISPR-EFS-GFP-rNRP-1 + VEGFA. We next performed blocking experiments to investigate the role of NaV1.7 channel as a downstream effector of VEGFA/NRP-1 signaling. If NaV1.7 is one of the targets of VEGFA/NRP-1, then knocking down NRP-1 in the presence of VEGFA and ProTx-II would not induce any changes in sodium influx. Co-application of ProTx-II did not produce an additional effect in peak sodium current density in cells with transfected pL-CRISPR-EFS-GFP-rNRP-1 + VEGFA (pL-CRISPR-EFS-GFP-rNRP-1+ VEGFA: −165.3 ± 37.2 pA/pF; pL-CRISPR-EFS-GFP-rNRP-1 + VEGFA + ProTx-II: −201.1 ± 42.4 pA/pF; p=0.9261; Figure 4C and Table S1). This suggests that VEGFA/NRP-1 and ProTx-II share a common target, NaV1.7 channels. No statistical difference was observed in $V_{1/2}$ or k for activation and inactivation (Figure 4D and Table S2). ProTx-II did not induce a prototypical rightward shift of half-voltage of activation [58] in these neurons as it was likely conflated by a rightward shift caused by VEGFA (compare Figure 3D with 4D). These data show that VEGFA-induced increase in sodium current density is mediated by NaV1.7 channels.

3.5 NRP-1 knockdown prevents VEGFA-mediated increase in calcium influx through CaV2.2 channels

As CaV2.2 channels are also a downstream targets of VEGFA/NRP-1 signaling in sensory neurons [45], we explored if facilitation of CaV2.2 currents by VEGFA was affected by NRP-1 silencing. We focused on these channels because of their relevance in neurotransmitter release and their participation in DRG neuron excitability [62]. To isolated CaV2.2 currents from small-to-medium sized DRG neurons, whole-cell patch-clamp recordings were performed in the presence of a cocktail of toxins and blockers (see Methods) that inhibit all other subtypes of voltage-gated calcium channels (L-, P/Q-, R-, and T-type) present in sensory neurons. Two days after transfecting DRGs with gRNA/Cas9 plasmids, we recorded currents through CaV2.2 channels. Figure 5A shows representative families of calcium currents evoked by depolarizing pulses from −70 mV to +60 mV in 10 mV increments. Treatment of pL-CRISPR-EFS-GFP with VEGFA (1 nM) enhanced CaV2.2 current density (pL-CRISPR-EFS-GFP: −27.93 ± 3.1 pA/pF; pL-CRISPR-EFS-GFP + VEGFA: −42.34 ± 4.2 pA/pF; p=0.0339; Figure 5B and C and Table S1). Indeed, VEGFA-mediated increase in CaV2.2 calcium current density was prevented when NRP-1 expression was edited (pL-CRISPR-EFS-GFP + VEGFA: −42.34 ± 4.2 pA/pF; pL-CRISPR-EFS-GFP-rNRP-1 + VEGFA: −28.14 ± 3.2 pA/pF; p=0.0035; Figure 5B and C and Table S1). Eliminating NRP-1 did not produce a significant change in constitutive CaV2.2 current density (pL-CRISPR-EFS-GFP: −27.9 ± 3.11 pA/pF; pL-CRISPR-EFS-GFP-rNRP-1: −23.67 ± 3.8 pA/pF; p=0.8603; Figure 5B and C and Table S1), which correlates with our previous report [45]. Importantly, there were no observable effects in the midpoint potential ($V_{1/2}$) and slope factor values (k) for activation and inactivation between the four groups (Figure 5D and Table S2). These results agree with our sodium current data (Figure 3 and 4) demonstrating that VEGFA requires NRP-1 as a co-receptor to induce the increase activity of voltage-gated calcium channels without affecting the channels' kinetics.

3.6 Voltage-gated potassium channels are not involved in VEGFA/NRP-1 signaling pathway

Voltage-gated potassium channels are critical modulators of neuronal excitability in the central and peripheral nervous systems [30]. DRG membrane hyperexcitability due to the loss of function of voltage-gated K^+ channels is an important mechanism underlying pain [14; 61]. Therefore, to assess if K^+ channels are targets of VEGFA/NRP-1 signaling pathway we used whole-cell patch-clamp recordings. Typical families of K^+ fast inactivating IK_A and slowly inactivating IK_S currents from DRG neurons are shown in Figure 6A. Incubation of pL-CRISPR-EFS-GFP-transfected sensory neurons with 1 nM of VEGFA did not produce any changes on IK_A current (Figure 6A), current density (Figure 6B), peak current densities (Figure 6C) nor on IK_S current densities (Figure 6D–E), when compared to cells transfected with control plasmid with Cas9 (IK_A - pL-CRISPR-EFS-GFP: 154.0 ± 25.62 pA/pF; pL-CRISPR-EFS-GFP + VEGFA: 128.7 ± 18.52 pA/pF; p>0.9999; IK_S - pL-CRISPR-EFS-GFP: 88.06 ± 14.79 pA/pF; pL-CRISPR-EFS-GFP + VEGFA: 89.09 ± 13.85 pA/pF; p>0.9999; Figure 6C and E and Table S1). Similarly, knocking down NRP-1 alone or in the presence of VEGFA did not alter potassium efflux through these channels (Figure 6C and E). These data show that voltage-gated potassium channels are not the downstream targets of VEGFA/NRP-1 signaling in DRG neurons.

3.7 Elimination of NRP-1 reduces VEGFA-mediated increase of the frequency of spontaneous excitatory postsynaptic currents in the lumbar dorsal horn

The task of integrating sensory data from DRG neurons, which react to classes of noxious and non-noxious stimuli, falls on the spinal cord. Complex circuits including excitatory and inhibitory interneurons filter this incoming information before transmitting it to various brain areas, including those in charge of pain perception [67]. Inhibiting NRP-1 signaling with EG00229 restores normalcy to the VEGFA-mediated increase of synaptic activity in the lumbar dorsal horn of the spinal cord [45]. To determine if VEGFA-enhanced neurotransmission is affected by deletion of NRP-1, we performed electrophysiological recordings in the whole-cell configuration mode to measure spontaneous excitatory postsynaptic currents (sEPSCs) of neurons in the *substantia gelatinosa* (SG) region of the lumbar dorsal horn of young rats (p10–15) two days post-intrathecal injections of the gRNA with Cas9 plasmids. Transfected neurons were identified by detection of GFP fluorescence co-expressed by these plasmids. To isolate spontaneous excitatory currents, we blocked the inhibitory component of the signal by acutely perfusing blockers of the GABAergic and glycinergic currents (bicuculline and strychnine, respectively). We added VEGFA (1 nM) acutely to the spinal cord slices to induce the increase in frequency observed previously [45]. Representative traces of sEPSCs from slices cut from rats transfected either with pL-CRISPR-EFS-GFP or pL-CRISPR-EFS-GFP-rNRP-1 plasmid in the absence or presence of VEGFA are shown in Figure 7A. Addition of VEGFA to the recording solution resulted in an increase of the frequency of sEPSCs compared to control slices without VEGFA (pL-CRISPR-EFS-GFP: 0.905 ± 0.269 Hz; pL-CRISPR-EFS-GFP + VEGFA: 3.122 ± 0.511 Hz; p=0.0005; Figure 7B and Table S1). The amplitude of sEPSCs was not changed by the different treatments (Figure 7C and Table S1). Next, we injected a cohort of young rats with pL-CRISPR-EFS-GFP-rNRP-1 and recorded sEPSCs from slices prepared 2 days later. Representative traces are shown in Figure 7A. When compared to control, we found no significant difference in both the frequency (Figure 7B and Table S1) nor the amplitude of sEPSCs (Figure 7C and Table S1), showing that NRP-1 deletion does not impact physiological synaptic transmission in the SDH. Consistent with these findings, frequency of sEPSCs of neurons in slices from pL-CRISPR-EFS-GFP-rNRP-1-transfected rats were significantly lower than those of the pL-CRISPR-EFS-GFP-transfected rats perfused with VEGFA (pL-CRISPR-EFS-GFP + VEGFA: 3.122 ± 0.511 Hz; pL-CRISPR-EFS-GFP-rNRP-1: 0.735 ± 0.133 Hz; p<0.0001; Figure 7B and Table S1). Importantly, when NRP-1 expression was deleted, adding VEGFA to the preparation did not increase neurotransmission (pL-CRISPR-EFS-GFP-rNRP-1: 0.735 ± 0.133 Hz; pL-CRISPR-EFS-GFP-rNRP-1 + VEGFA: 1.561 ± 0.251 Hz; p=0.3267; Figure 7B and Table S1). Indeed, sEPSC frequencies were significantly lower despite the addition of VEGFA to the pL-CRISPR-EFS-GFP-rNRP-1-transfected slices compared to the pL-CRISPR-EFS-GFP-transfected slices treated with VEGFA (pL-CRISPR-EFS-GFP + VEGFA: 3.122 ± 0.511 Hz; pL-CRISPR-EFS-GFP-rNRP-1 + VEGFA: 1.561 ± 0.251 Hz; p=0.0080; Figure 7B and Table S1). Together, these results show that VEGFA-mediated increased neurotransmission in the SDH is blocked by the deletion of NRP-1, which is concordant with previous results obtained through selective pharmacological antagonism of NRP-1 [45]. Therefore, VEGFA-mediated neurotransmission in the SDH depends on the availability

of NRP-1, a conclusion confirmed with CRISPR/Cas9 editing of NRP-1, supporting the hypothesis that NRP-1 is the target of VEGFA in spinal neurotransmission.

3.8 NRP-1 knockdown reverses neuropathic pain in rats

We showed above that NRP-1 gene editing reduces VEGFA-mediated increase in spinal neurotransmission (Figure 7). To support the pathophysiological role of NRP-1 during pain signaling *in vivo*, we next tested the importance of this receptor in a model of neuropathic pain. For this, we chose the L5/L6 spinal nerve ligation (SNL) model of neuropathic pain [26], one of the most widely used models known to induce both spontaneous and evoked pain (hyperalgesia and allodynia) in the absence of autotomy [3; 9]. Before surgeries (BL), we assessed PWT to mechanical stimuli and PWL to heat stimuli in male and female rats (Figure 8). The operation resulted in long-lasting behavioral signs of mechanical allodynia (Figure 8A, B, C, D) and heat hyperalgesia (Figure 8E, F, G, H) fourteen days after SNL (pre-injection timepoint). Next, control gRNA with Cas9 and NRP-1 gRNA with Cas9 lentiviruses ($1x10^6$ live particles in 5 μL) were intrathecally (i.t.) injected into the lumbar region of the rats' spinal cords. We measured PWTs (Figure 8A and C) and PWLs (Figure 8E and G) at 5, 10-, 15-, 20- and 25-days post-injection. As represented in Figures 8A and C, knocking-down NRP-1 partially reversed SNL-induced mechanical allodynia from 5 to 15 days after lentiviral injections in male rats (AUC - control gRNA with Cas9 lentivirus: 10.62 ± 3.037; NRP-1 gRNA Cas9 lentivirus: 23.42 ± 4.432; p=0.0486), and from 5 to 10 days after lentiviral injections in female rats (AUC - control gRNA Cas9 lentivirus: 4.834 ± 1.184; NRP-1 gRNA Cas9 lentivirus: 16.63 ± 4.444; p=0.0262; Figures 8B and D; Table S1). Figures 8E and G show that silencing NRP-1 after inducing neuropathic pain, also diminished thermal hypersensitivity by increasing the PWL from 5 to 15 days after lentiviral injections in male (AUC - control gRNA with Cas9 lentivirus: 9.334 ± 1.193; NRP-1 gRNA Cas9 lentivirus: 18.61 ± 3.851; p=0.0303), and female rats (AUC - control gRNA Cas9 lentivirus: 14.80 ± 3.503; NRP-1 gRNA Cas9 lentivirus: 41.27 ± 5.422; p=0.0022; Figures 8F and H; Table S1). These observations suggest that the lack of NRP-1 blunts mechanical allodynia and thermal hyperalgesia induced by nerve injury and show for the first time the relevance of NRP-1 in a neuropathic pain model.

4. Discussion

Ligand binding of membrane expressed receptor tyrosine kinases and their co-receptors initiate cascades that transduce extracellular signals into cellular actions. Here, we interrogated the function of NRP-1, a VEGFA co-receptor that complexes with VEGF Receptor 2 (VEGFR2), and that has promise as a clinically useful modulator of VEGF-mediated pain signaling. We report that *Nrp1* is expressed in peptidergic and non-peptidergic putative nociceptive sensory neurons. We specifically studied ligand-dependent effects on downstream targets involved in nociception. We conclusively identified that VEGFA engagement of the NRP-1/VEGFR2 complex leads to potentiation of ion channels involved in nociception and higher glutamatergic neurotransmission in the spinal cord that culminates in the development of pain-like behaviors. Further, we demonstrate a loss of VEGFA's pro-nociceptive actions in cells and animals after a partial knockout of NRP-1 via CRISPR/

Cas9 editing. We conclude that NRP-1 is necessary for the VEGFA-mediated increase of sensory neuron activity and development of pain-like behaviors.

VEGFs are involved in angiogenesis, vascular-related diseases [24], cancer-induced bone pain [15], neuropathic pain [41], and inflammatory conditions (rheumatoid arthritis and osteoarthritis [22; 65]). VEGFA modifies nociception by activating VEGFR2 and sensitizing peripheral nociceptive neurons [28]. The VEGFA family consists of different isoforms resulting from alternative splicing of exons 6, 7 and 8 [16]. The first VEGFA isoform described was $VEGFA_{165}$ and it has been extensively investigated for its anti-angiogenesis roles in cancer. VEGFA primarily signals via its cognate receptor tyrosine kinase VEGFR2. VEGFR2 is expressed in A and C fibers and its activity is increased during neuropathic pain [36]. The activity of VEGFR2 is regulated by an equilibrium between isoforms $VEGFA_{165a}$ and $VEGFA_{165b}$ [24]. In rats and mice, $VEGFA_{165a}$ and $VEGFA_{165b}$ have opposing effects on pain [28], with $VEGFA_{165a}$ being pro-nociceptive, and $VEGFA_{165b}$ being anti-nociceptive [28]. $VEGFA_{165a}$ sensitizes C fibers which leads to increased pain transmission and development of mechanical allodynia – an effect mediated by transient receptor potential vanilloid 1 (TRPV1) and TRPA1 channel activity [28]. On the other hand, the anti-angiogenic $VEGFA_{165b}$ suppresses TRPV1 and TRPA1 mediated activation of DRG sensory neurons, C fiber sensitization, and neuropathic pain [28]. It is the balance between these two splice isoforms that maintain the activity of nociceptive neurons, however, expression of the NRP-1 co-receptor also mediates this activity by potentiating this signaling [41; 71]. A membrane associated NRP-1 alternatively spliced isoform has also been identified, designated as NRP-1 (Δexon16), which lacks 51 nucleotides from exon 16 [56; 66]. Interestingly, NRP-1 (Δexon16) does not differ from the common full-length NRP1 in its binding to $VEGFA_{165}$, dimerization with VEGFR2 or regulation of $VEGFA_{165}$ signaling [66]. Thus, both NRP-1 and NRP-1(Δexon16) mediate VEGFA-induced signaling in a similar manner. Similarly, it is important to note that peripheral nerve injury increases the expression of VEGFA in the injured nerve. This up-regulated VEGF expression has been isolated to infiltrating macrophages and neutrophils [34]. Thus, we hypothesize that after neuropathic injury, infiltrating macrophages release VEGFA and drive nociceptor hyperactivity via NRP-1.

NRP-1 and its isoforms have been identified throughout the body. NRP-1 was initially described to be important in tumor genesis, with NRP-1 upregulation correlating to aggressive cancer phenotypes [31]. NRP-1 also has an emerging role in the sensory system [1]. NRP-1 is expressed in some neuronal structures, including hippocampus, cortex, cerebellum, olfactory bulb, spinal cord, and DRG neurons [18; 32; 55; 63]. Databases of deep RNA-sequencing (seq) data compiled by researchers from the University of Oxford, allow the visualization of *Nrp1* expression in different subpopulations of DRG neurons as (Peptidergic (*Calca*), C-Low Threshold Mechanoreceptors (*Th*), non-peptidergic (*Mrgprd*) nociceptors, Aβ- rapidly adapting (RA) + Aδ-LTMRs (*Ntrk2*), and general nociceptors (*Scn10a*). These data showed that *Nrp1* is present in various sensory neuron subtypes, which correlates with our findings showing that in sensory neurons, *Nrp1*-expressing neurons co-expressed calcitonin gene-related peptide (CGRP), as well as voltage-gated sodium channel marker NaV1.7. In our DRG sodium current recordings, some DRG populations were insensitive to VEGFA. A plausible explanation for this is that *Nrp1* is not present

in all DRG neurons (for example ~50% of *Calca*-expressing peptidergic neurons did not co-express *Nrp1* (Figure 1B)). Similarly, differential expression patterns of NaV channels could be contributing to this insensitivity to VEGFA. It could be possible that some sodium channels do not respond to VEGFA/NRP-1 signaling.

NRP-1 RNA and protein are up-regulated in the spinal cord after spinal cord injury and following dorsal root rhizotomy [1]. Similarly, peripheral axotomy increases NRP-1 expression in large-diameter DRG neurons [19]. The fact that both VEGFA [65] and NRP-1 [37] increase during pain, prompted us to study in more detail the relevance of NRP-1 as a co-receptor for VEGFA and its role in pain. In line with this, we show for the first time that silencing NRP-1 in the spinal cord of rats with neuropathic pain reverses nociceptive behaviors induced by nerve injury, arguing for a role of NRP-1 in chronic pain. Further, we found that the increase in sodium and calcium currents imposed by VEGFA was completely blocked by knocking-down NRP-1, corroborating the findings that the presence of NRP-1 co-receptor potentiates the effects of VEGFA [71]. Our working model also showed for the first time that NaV1.7 is mediating, in part, the increased activity of voltage-gated sodium channels by VEGFA. These results, together with the findings that CaV2.2 (N-type) calcium channel are also modulated by this pathway, suggests that the regulation of these ion channels through this axis could be targeted for development of pain therapeutics. A phase 1a/b clinical trial of NRP-1 antibody MNRP1685A/Vesencumab®, targeting the VEGFA-binding site of NRP-1, was well-tolerated in cancer patients [70]. While this antibody has not been evaluated in neuropathic pain, our preclinical work provides a rationale for targeting the VEGF-A/NRP-1 pro-nociceptive signaling axis in future clinical trials. MNRP1685A binds with high affinity to NRP-1 in mice, rats, cynomolgus monkeys, and humans (5–7 times higher than in other species), and modeling of its pharmacokinetic parameters suggest similar *in vivo* target engagement across all species [73]. Therefore, the likelihood of MNRP1685A/Vesencumab® being fast-tracked to clinical trials is a potentially exciting and innovative outcome of our findings.

Since NRP-1 (Δexon16) is only present in endothelial cells, astrocytes, and tumor cell lines [66], it is plausible that our approach of knocking down NRP-1 in the sensory system is not being affected by the expression of this isoform. Despite reports showing that VEGFA inhibits outward delayed-rectifier potassium currents in hippocampal neurons [74], we observed that the actions of VEGFA on NRP-1 do not involve fast inactivating IK_A and slowly inactivating IK_S channels. Our data does not rule out an effect of this signaling pathway on other voltage-gated ion channels, however, our results do validate that the resulting decrease in neurotransmission in the spinal cord could be arising, in part, from the decreased activity of NaV1.7 and CaV2.2 channels in sensory neurons. These results are consistent with our findings that pain induced by VEGFA is blocked by pharmacological inhibition of NRP-1, and that NRP-1 antagonism reverses SNI-induced mechanical allodynia [45]. Identification and characterization of the signaling cascade downstream of VEGFA/NRP-1 axis awaits further work. Activation of NRP-1 with VEGFA165a elicits NRP-1–mediated VEGFR-2 recycling through early endosomal and recycling vesicles, while activation by the VEGFA165b isoform directs VEGFR2 to a degradative pathway [2]. How these endocytic and recycling pathways intersect with downstream signaling and/or couple to ion channels is unknown. Another question, not

tested here, is if the NRP-1 interacting protein synectin [7] is required to mediate the effects of VEGFA activation onto ion channels, synaptic transmission, and nociception.

Neuropilins also serve as co-receptors for class III semaphorin (Sema3) family of axon guidance molecules [53]. In chronic neuropathic pain, expression of both Sema3A and VEGFA is increased [38]. However, we previously reported that Sema3A did not increase DRG neuron spontaneous firing [45], despite previous reports linking Sema3A expression to low back [68] and cancer-induced bone [40] pain. The ligand prioritization of Sema3A may explain this seeming incongruity as Sema3A binds to a different pocket on NRP-1 [51] than VEGFA [52] and signals through a different co-receptor (PlexinA1). VEGF-A165 induces clathrin-dependent endocytosis, whereas sema3C induces lipid raft−dependent endocytosis [57]. The Kuner group reported that intraplantar injection of neutralizing antibodies directed against NRP-1, which function as VEGFR co-receptors in some systems [48], did not inhibit VEGFA-induced nociceptive sensitization [59]. While these results may seem at odds with our findings, potential explanations include: the route of administration (intraplantar versus intrathecal in our study), the kinetics of binding of the antibody to NRP1 may be slower than that of VEGFA, and use of polyclonal antibody and lack of demonstration of antibody mediated neutralization of VEGFA.

In conclusion, our pre-clinical data show that NRP-1 is expressed in putative nociceptive primary sensory neurons. Further, we demonstrate that CRISPR-mediated reduction of NRP-1: (*i*) prevents VEGFA-induced sensory neuron hyperactivity, (*ii*) prevents VEGFA-induced increase in spinal neurotransmission, and (*iii*) reduces nerve injury-induced mechanical and thermal hypersensitivity. Overall, our results converge on identification of NRP-1 as a co-receptor that is indispensable for the pro-nociceptive actions of VEGFA and that is a promising pharmacotherapeutic target for the treatment of pain.

Supplementary Material

Refer to Web version on PubMed Central for supplementary material.

Acknowledgments

This study was supported by National Institutes of Health awards (NS098772, NS120663, NS122545, and DA042852 to R.K.; NS102722, DE026806, R01DE029951, and DK118971 to N.W.B.), and Department of Defense grants (W81XWH1810431, W81XWH2210238 to N.W.B). R.K. is the founder of Regulonix LLC, a company developing nonopioid drugs for chronic pain. In addition, R.K., has patents US10287334 (non-narcotic CRMP2 peptides targeting sodium channels for chronic pain) and US10441586 (SUMOylation inhibitors and uses thereof) issued to Regulonix LLC. N.W.B is a founding scientist of Endosome Therapeutics Inc. Research in N.W.B.'s laboratory is funded, in part, by Takeda Pharmaceuticals International. All other authors declare no competing interests.

Data availability statement:

The dataset supporting the conclusions of this article are included within the article and the additional supplementary file.

References

[1]. Agudo M, Robinson M, Cafferty W, Bradbury EJ, Kilkenny C, Hunt SP, McMahon SB. Regulation of neuropilin 1 by spinal cord injury in adult rats. Mol Cell Neurosci 2005;28(3):475–484. [PubMed: 15737738]

[2]. Ballmer-Hofer K, Andersson AE, Ratcliffe LE, Berger P. Neuropilin-1 promotes VEGFR-2 trafficking through Rab11 vesicles thereby specifying signal output. Blood 2011;118(3):816–826. [PubMed: 21586748]

[3]. Tests Barrot M. and models of nociception and pain in rodents. Neuroscience 2012;211:39–50. [PubMed: 22244975]

[4]. Basbaum AI, Bautista DM, Scherrer G, Julius D. Cellular and molecular mechanisms of pain. Cell 2009;139(2):267–284. [PubMed: 19837031]

[5]. Boinon L, Yu J, Madura CL, Chefdeville A, Feinstein DL, Moutal A, Khanna R. Conditional knockout of CRMP2 in neurons, but not astrocytes, disrupts spinal nociceptive neurotransmission to control the initiation and maintenance of chronic neuropathic pain. Pain 2022;163(2):e368–e381. [PubMed: 35029600]

[6]. Brittain JM, Piekarz AD, Wang Y, Kondo T, Cummins TR, Khanna R. An atypical role for collapsin response mediator protein 2 (CRMP-2) in neurotransmitter release via interaction with presynaptic voltage-gated calcium channels. J Biol Chem 2009;284(45):31375–31390. [PubMed: 19755421]

[7]. Cai H, Reed RR. Cloning and characterization of neuropilin-1-interacting protein: a PSD-95/Dlg/ZO-1 domain-containing protein that interacts with the cytoplasmic domain of neuropilin-1. J Neurosci 1999;19(15):6519–6527. [PubMed: 10414980]

[8]. Cantuti-Castelvetri L, Ojha R, Pedro LD, Djannatian M, Franz J, Kuivanen S, van der Meer F, Kallio K, Kaya T, Anastasina M, Smura T, Levanov L, Szirovicza L, Tobi A, Kallio-Kokko H, Österlund P, Joensuu M, Meunier FA, Butcher SJ, Winkler MS, Mollenhauer B, Helenius A, Gokce O, Teesalu T, Hepojoki J, Vapalahti O, Stadelmann C, Balistreri G, Simons M. Neuropilin-1 facilitates SARS-CoV-2 cell entry and infectivity. Science 2020;370(6518):856–860. [PubMed: 33082293]

[9]. Challa SR. Surgical animal models of neuropathic pain: Pros and Cons. Int J Neurosci 2015;125(3):170–174. [PubMed: 24831263]

[10]. Chaplan SR, Bach FW, Pogrel JW, Chung JM, Yaksh TL. Quantitative assessment of tactile allodynia in the rat paw. J Neurosci Methods 1994;53(1):55–63. [PubMed: 7990513]

[11]. Chekol Abebe E, Mengie Ayele T, Tilahun Muche Z, Asmamaw Dejenie T. Neuropilin 1: A Novel Entry Factor for SARS-CoV-2 Infection and a Potential Therapeutic Target. Biologics 2021;15:143–152. [PubMed: 33986591]

[12]. Daly JL, Simonetti B, Klein K, Chen KE, Williamson MK, Antón-Plágaro C, Shoemark DK, Simón-Gracia L, Bauer M, Hollandi R, Greber UF, Horvath P, Sessions RB, Helenius A, Hiscox JA, Teesalu T, Matthews DA, Davidson AD, Collins BM, Cullen PJ, Yamauchi Y. Neuropilin-1 is a host factor for SARS-CoV-2 infection. Science 2020;370(6518):861–865. [PubMed: 33082294]

[13]. Dib-Hajj SD, Yang Y, Black JA, Waxman SG. The Na(V)1.7 sodium channel: from molecule to man. Nat Rev Neurosci 2013;14(1):49–62. [PubMed: 23232607]

[14]. Du X, Gamper N. Potassium channels in peripheral pain pathways: expression, function and therapeutic potential. Curr Neuropharmacol 2013;11(6):621–640. [PubMed: 24396338]

[15]. Fan LJ, Kan HM, Chen XT, Sun YY, Chen LP, Shen W. Vascular endothelial growth factor-A/vascular endothelial growth factor2 signaling in spinal neurons contributes to bone cancer pain. Mol Pain 2022;18:17448069221075891.

[16]. Ferrara N Vascular endothelial growth factor: basic science and clinical progress. Endocr Rev 2004;25(4):581–611. [PubMed: 15294883]

[17]. Francois-Moutal L, Dustrude ET, Wang Y, Brustovetsky T, Dorame A, Ju W, Moutal A, Perez-Miller S, Brustovetsky N, Gokhale V, Khanna M, Khanna R. Inhibition of the Ubc9 E2 SUMO-conjugating enzyme-CRMP2 interaction decreases NaV1.7 currents and reverses experimental neuropathic pain. Pain 2018;159(10):2115–2127. [PubMed: 29847471]

[18]. Gavazzi I Semaphorin-neuropilin-1 interactions in plasticity and regeneration of adult neurons. Cell Tissue Res 2001;305(2):275–284. [PubMed: 11545265]

[19]. Gavazzi I, Stonehouse J, Sandvig A, Reza JN, Appiah-Kubi LS, Keynes R, Cohen J. Peripheral, but not central, axotomy induces neuropilin-1 mRNA expression in adult large diameter primary sensory neurons. J Comp Neurol 2000;423(3):492–499. [PubMed: 10870088]

[20]. Ghez D, Lepelletier Y, Lambert S, Fourneau J-M, Blot V, Janvier S, Arnulf B, Endert PMv, Heveker N, Pique C, Hermine O. Neuropilin-1 Is Involved in Human T-Cell Lymphotropic Virus Type 1 Entry. Journal of Virology 2006;80(14):6844–6854. [PubMed: 16809290]

[21]. Guo HF, Vander Kooi CW. Neuropilin Functions as an Essential Cell Surface Receptor. J Biol Chem 2015;290(49):29120–29126. [PubMed: 26451046]

[22]. Hamilton JL, Nagao M, Levine BR, Chen D, Olsen BR, Im HJ. Targeting VEGF and Its Receptors for the Treatment of Osteoarthritis and Associated Pain. J Bone Miner Res 2016;31(5):911–924. [PubMed: 27163679]

[23]. Hargreaves K, Dubner R, Brown F, Flores C, Joris J. A new and sensitive method for measuring thermal nociception in cutaneous hyperalgesia. Pain 1988;32(1):77–88. [PubMed: 3340425]

[24]. Harper SJ, Bates DO. VEGF-A splicing: the key to anti-angiogenic therapeutics? Nat Rev Cancer 2008;8(11):880–887. [PubMed: 18923433]

[25]. Heckl D, Kowalczyk MS, Yudovich D, Belizaire R, Puram RV, McConkey ME, Thielke A, Aster JC, Regev A, Ebert BL. Generation of mouse models of myeloid malignancy with combinatorial genetic lesions using CRISPR-Cas9 genome editing. Nat Biotechnol 2014;32(9):941–946. [PubMed: 24952903]

[26]. Ho Kim S, Mo Chung J. An experimental model for peripheral neuropathy produced by segmental spinal nerve ligation in the rat. Pain 1992;50(3):355–363. [PubMed: 1333581]

[27]. Hulse RP. Role of VEGF-A in chronic pain. Oncotarget 2017;8(7):10775–10776. [PubMed: 28099925]

[28]. Hulse RP, Beazley-Long N, Hua J, Kennedy H, Prager J, Bevan H, Qiu Y, Fernandes ES, Gammons MV, Ballmer-Hofer K, Gittenberger de Groot AC, Churchill AJ, Harper SJ, Brain SD, Bates DO, Donaldson LF. Regulation of alternative VEGF-A mRNA splicing is a therapeutic target for analgesia. Neurobiol Dis 2014;71:245–259. [PubMed: 25151644]

[29]. Jarvis A, Allerston CK, Jia H, Herzog B, Garza-Garcia A, Winfield N, Ellard K, Aqil R, Lynch R, Chapman C, Hartzoulakis B, Nally J, Stewart M, Cheng L, Menon M, Tickner M, Djordjevic S, Driscoll PC, Zachary I, Selwood DL. Small molecule inhibitors of the neuropilin-1 vascular endothelial growth factor A (VEGF-A) interaction. Journal of medicinal chemistry 2010;53(5):2215–2226. [PubMed: 20151671]

[30]. Johnston J, Forsythe ID, Kopp-Scheinpflug C. Going native: voltage-gated potassium channels controlling neuronal excitability. J Physiol 2010;588(Pt 17):3187–3200. [PubMed: 20519310]

[31]. Jubb AM, Strickland LA, Liu SD, Mak J, Schmidt M, Koeppen H. Neuropilin-1 expression in cancer and development. J Pathol 2012;226(1):50–60. [PubMed: 22025255]

[32]. Kawasaki T, Bekku Y, Suto F, Kitsukawa T, Taniguchi M, Nagatsu I, Nagatsu T, Itoh K, Yagi T, Fujisawa H. Requirement of neuropilin 1-mediated Sema3A signals in patterning of the sympathetic nervous system. Development 2002;129(3):671–680. [PubMed: 11830568]

[33]. Khanna R, Yu J, Yang X, Moutal A, Chefdeville A, Gokhale V, Shuja Z, Chew LA, Bellampalli SS, Luo S, François-Moutal L, Serafini MJ, Ha T, Perez-Miller S, Park KD, Patwardhan AM, Streicher JM, Colecraft HM, Khanna M. Targeting the CaVα-CaVβ interaction yields an antagonist of the N-type CaV2.2 channel with broad antinociceptive efficacy. Pain 2019;160(7):1644–1661. [PubMed: 30933958]

[34]. Kiguchi N, Kobayashi Y, Kadowaki Y, Fukazawa Y, Saika F, Kishioka S. Vascular endothelial growth factor signaling in injured nerves underlies peripheral sensitization in neuropathic pain. J Neurochem 2014;129(1):169–178. [PubMed: 24304382]

[35]. Li Y, North RY, Rhines LD, Tatsui CE, Rao G, Edwards DD, Cassidy RM, Harrison DS, Johansson CA, Zhang H, Dougherty PM. DRG Voltage-Gated Sodium Channel 1.7 Is Upregulated in Paclitaxel-Induced Neuropathy in Rats and in Humans with Neuropathic Pain. J Neurosci 2018;38(5):1124–1136. [PubMed: 29255002]

[36]. Lin J, Li G, Den X, Xu C, Liu S, Gao Y, Liu H, Zhang J, Li X, Liang S. VEGF and its receptor-2 involved in neuropathic pain transmission mediated by P2X(2)(/)(3) receptor of primary sensory neurons. Brain Res Bull 2010;83(5):284–291. [PubMed: 20705122]

[37]. Lindholm T, Risling M, Carlstedt T, Hammarberg H, Wallquist W, Cullheim S, Sköld MK. Expression of Semaphorins, Neuropilins, VEGF, and Tenascins in Rat and Human Primary Sensory Neurons after a Dorsal Root Injury. Frontiers in Neurology 2017;8.

[38]. Lindholm T, Risling M, Carlstedt T, Hammarberg H, Wallquist W, Cullheim S, Sköld MK. Expression of Semaphorins, Neuropilins, VEGF, and Tenascins in Rat and Human Primary Sensory Neurons after a Dorsal Root Injury. Frontiers in Neurology 2017;8(49).

[39]. Ma H, Marti-Gutierrez N, Park SW, Wu J, Lee Y, Suzuki K, Koski A, Ji D, Hayama T, Ahmed R, Darby H, Van Dyken C, Li Y, Kang E, Park AR, Kim D, Kim ST, Gong J, Gu Y, Xu X, Battaglia D, Krieg SA, Lee DM, Wu DH, Wolf DP, Heitner SB, Belmonte JCI, Amato P, Kim JS, Kaul S, Mitalipov S. Correction of a pathogenic gene mutation in human embryos. Nature 2017;548(7668):413–419. [PubMed: 28783728]

[40]. Maeda T, Yamada D, Kawahara K. Cancer pain relief achieved by disrupting tumor-driven semaphorin 3A signaling in mice. Neuroscience letters 2016;632:147–151. [PubMed: 27592511]

[41]. Makinen T, Olofsson B, Karpanen T, Hellman U, Soker S, Klagsbrun M, Eriksson U, Alitalo K. Differential binding of vascular endothelial growth factor B splice and proteolytic isoforms to neuropilin-1. J Biol Chem 1999;274(30):21217–21222. [PubMed: 10409677]

[42]. McCarthy KF, Connor TJ, McCrory C. Cerebrospinal fluid levels of vascular endothelial growth factor correlate with reported pain and are reduced by spinal cord stimulation in patients with failed back surgery syndrome. Neuromodulation 2013;16(6):519–522; discussion 522. [PubMed: 23136965]

[43]. Moutal A, Cai S, Luo S, Voisin R, Khanna R. CRMP2 is necessary for Neurofibromatosis type 1 related pain. Channels (Austin) 2018;12(1):47–50. [PubMed: 28837387]

[44]. Moutal A, Martin LF, Boinon L, Gomez K, Ran D, Zhou Y, Stratton HJ, Cai S, Luo S, Gonzalez KB, Perez-Miller S, Patwardhan A, Ibrahim MM, Khanna R. SARS-CoV-2 spike protein co-opts VEGF-A/neuropilin-1 receptor signaling to induce analgesia. Pain 2021;162(1):243–252. [PubMed: 33009246]

[45]. Moutal A, Martin LF, Boinon L, Gomez K, Ran D, Zhou Y, Stratton HJ, Cai S, Luo S, Gonzalez KB, Perez-Miller S, Patwardhan A, Ibrahim MM, Khanna R. SARS-CoV-2 Spike protein co-opts VEGF-A/Neuropilin-1 receptor signaling to induce analgesia. Pain 2021;162:243–252. [PubMed: 33009246]

[46]. Moutal A, Sun L, Yang X, Li W, Cai S, Luo S, Khanna R. CRMP2-Neurofibromin Interface Drives NF1-related Pain. Neuroscience 2018;381:79–90. [PubMed: 29655575]

[47]. Moutal A, Yang X, Li W, Gilbraith KB, Luo S, Cai S, Francois-Moutal L, Chew LA, Yeon SK, Bellampalli SS, Qu C, Xie JY, Ibrahim MM, Khanna M, Park KD, Porreca F, Khanna R. CRISPR/Cas9 editing of Nf1 gene identifies CRMP2 as a therapeutic target in neurofibromatosis type 1-related pain that is reversed by (S)-Lacosamide. Pain 2017;158(12):2301–2319. [PubMed: 28809766]

[48]. Olsson AK, Dimberg A, Kreuger J, Claesson-Welsh L. VEGF receptor signalling - in control of vascular function. Nat Rev Mol Cell Biol 2006;7(5):359–371. [PubMed: 16633338]

[49]. Orazov MR, Nosenko EN, Radzinsky VE, Khamoshina MB, Lebedeva MG, Sounov MA. Proangiogenic features in chronic pelvic pain caused by adenomyosis. Gynecol Endocrinol 2016;32(sup2):7–10. [PubMed: 27759451]

[50]. Orlova IA, Alexander GM, Qureshi RA, Sacan A, Graziano A, Barrett JE, Schwartzman RJ, Ajit SK. MicroRNA modulation in complex regional pain syndrome. J Transl Med 2011;9:195. [PubMed: 22074333]

[51]. Palodetto B, da Silva Santos Duarte A, Rodrigues Lopes M, Adolfo Corrocher F, Marconi Roversi F, Soares Niemann F, Priscila Vieira Ferro K, Leda Figueiredo Longhini A, Melo Campos P, Favaro P, Teresinha Olalla Saad S. SEMA3A partially reverses VEGF effects through binding to neuropilin-1. Stem Cell Research 2017;22:70–78. [PubMed: 28636974]

[52]. Parker MW, Xu P, Li X, Vander Kooi CW. Structural basis for selective vascular endothelial growth factor-A (VEGF-A) binding to neuropilin-1. The Journal of biological chemistry 2012;287(14):11082–11089. [PubMed: 22318724]

[53]. Pellet-Many C, Frankel P, Jia H, Zachary I. Neuropilins: structure, function and role in disease. Biochem J 2008;411(2):211–226. [PubMed: 18363553]

[54]. Piekarz AD, Due MR, Khanna M, Wang B, Ripsch MS, Wang R, Meroueh SO, Vasko MR, White FA, Khanna R. CRMP-2 peptide mediated decrease of high and low voltage-activated calcium channels, attenuation of nociceptor excitability, and anti-nociception in a model of AIDS therapy-induced painful peripheral neuropathy. Mol Pain 2012;8:54. [PubMed: 22828369]

[55]. Reza JN, Gavazzi I, Cohen J. Neuropilin-1 is expressed on adult mammalian dorsal root ganglion neurons and mediates semaphorin3a/collapsin-1-induced growth cone collapse by small diameter sensory afferents. Mol Cell Neurosci 1999;14(4–5):317–326. [PubMed: 10588387]

[56]. Rossignol M, Gagnon ML, Klagsbrun M. Genomic organization of human neuropilin-1 and neuropilin-2 genes: identification and distribution of splice variants and soluble isoforms. Genomics 2000;70(2):211–222. [PubMed: 11112349]

[57]. Salikhova A, Wang L, Lanahan AA, Liu M, Simons M, Leenders WP, Mukhopadhyay D, Horowitz A. Vascular endothelial growth factor and semaphorin induce neuropilin-1 endocytosis via separate pathways. Circ Res 2008;103(6):e71–79. [PubMed: 18723443]

[58]. Schmalhofer WA, Calhoun J, Burrows R, Bailey T, Kohler MG, Weinglass AB, Kaczorowski GJ, Garcia ML, Koltzenburg M, Priest BT. ProTx-II, a selective inhibitor of NaV1.7 sodium channels, blocks action potential propagation in nociceptors. Mol Pharmacol 2008;74(5):1476–1484. [PubMed: 18728100]

[59]. Selvaraj D, Gangadharan V, Michalski Christoph W, Kurejova M, Stösser S, Srivastava K, Schweizerhof M, Waltenberger J, Ferrara N, Heppenstall P, Shibuya M, Augustin Hellmut G, Kuner R. A Functional Role for VEGFR1 Expressed in Peripheral Sensory Neurons in Cancer Pain. Cancer Cell 2015;27(6):780–796. [PubMed: 26058077]

[60]. Selvaraj D, Gangadharan V, Michalski CW, Kurejova M, Stösser S, Srivastava K, Schweizerhof M, Waltenberger J, Ferrara N, Heppenstall P, Shibuya M, Augustin HG, Kuner R. A Functional Role for VEGFR1 Expressed in Peripheral Sensory Neurons in Cancer Pain. Cancer Cell 2015;27(6):780–796. [PubMed: 26058077]

[61]. Smith PA. K(+) Channels in Primary Afferents and Their Role in Nerve Injury-Induced Pain. Front Cell Neurosci 2020;14:566418. [PubMed: 33093824]

[62]. Snutch TP. Targeting chronic and neuropathic pain: the N-type calcium channel comes of age. NeuroRx 2005;2(4):662–670. [PubMed: 16489373]

[63]. Solowska JM, Mazurek A, Weinberger L, Baird DH. Pontocerebellar axon guidance: neuropilin-1- and semaphorin 3A-sensitivity gradients across basilar pontine nuclei and semaphorin 3A variation across cerebellum. Mol Cell Neurosci 2002;21(2):266–284. [PubMed: 12401447]

[64]. Takahashi T, Fournier A, Nakamura F, Wang LH, Murakami Y, Kalb RG, Fujisawa H, Strittmatter SM. Plexin-neuropilin-1 complexes form functional semaphorin-3A receptors. Cell 1999;99(1):59–69. [PubMed: 10520994]

[65]. Takano S, Uchida K, Inoue G, Matsumoto T, Aikawa J, Iwase D, Mukai M, Miyagi M, Takaso M. Vascular endothelial growth factor expression and their action in the synovial membranes of patients with painful knee osteoarthritis. BMC Musculoskelet Disord 2018;19(1):204. [PubMed: 29945585]

[66]. Tao Q, Spring SC, Terman BI. Characterization of a new alternatively spliced neuropilin-1 isoform. Angiogenesis 2003;6(1):39–45. [PubMed: 14517403]

[67]. Todd AJ. Neuronal circuitry for pain processing in the dorsal horn. Nat Rev Neurosci 2010;11(12):823–836. [PubMed: 21068766]

[68]. Tolofari SK, Richardson SM, Freemont AJ, Hoyland JA. Expression of semaphorin 3A and its receptors in the human intervertebral disc: potential role in regulating neural ingrowth in the degenerate intervertebral disc. Arthritis research & therapy 2010;12(1):R1. [PubMed: 20051117]

[69]. Verheyen A, Peeraer E, Nuydens R, Dhondt J, Poesen K, Pintelon I, Daniels A, Timmermans JP, Meert T, Carmeliet P, Lambrechts D. Systemic anti-vascular endothelial growth factor therapies

induce a painful sensory neuropathy. Brain : a journal of neurology 2012;135(Pt 9):2629–2641. [PubMed: 22734125]

[70]. Weekes CD, Beeram M, Tolcher AW, Papadopoulos KP, Gore L, Hegde P, Xin Y, Yu R, Shih LM, Xiang H, Brachmann RK, Patnaik A. A phase I study of the human monoclonal anti-NRP1 antibody MNRP1685A in patients with advanced solid tumors. Invest New Drugs 2014;32(4):653–660. [PubMed: 24604265]

[71]. Whitaker GB, Limberg BJ, Rosenbaum JS. Vascular endothelial growth factor receptor-2 and neuropilin-1 form a receptor complex that is responsible for the differential signaling potency of VEGF(165) and VEGF(121). J Biol Chem 2001;276(27):25520–25531. [PubMed: 11333271]

[72]. Xie JY, Chew LA, Yang X, Wang Y, Qu C, Wang Y, Federici LM, Fitz SD, Ripsch MS, Due MR, Moutal A, Khanna M, White FA, Vanderah TW, Johnson PL, Porreca F, Khanna R. Sustained relief of ongoing experimental neuropathic pain by a CRMP2 peptide aptamer with low abuse potential. Pain 2016;157(9):2124–2140. [PubMed: 27537210]

[73]. Xin Y, Bai S, Damico-Beyer LA, Jin D, Liang WC, Wu Y, Theil FP, Joshi A, Lu Y, Lowe J, Maia M, Brachmann RK, Xiang H. Anti-neuropilin-1 (MNRP1685A): unexpected pharmacokinetic differences across species, from preclinical models to humans. Pharmaceutical research 2012;29(9):2512–2521. [PubMed: 22707361]

[74]. Xu JY, Zheng P, Shen DH, Yang SZ, Zhang LM, Huang YL, Sun FY. Vascular endothelial growth factor inhibits outward delayed-rectifier potassium currents in acutely isolated hippocampal neurons. Neuroscience 2003;118(1):59–67. [PubMed: 12676137]

[75]. Yu J, Moutal A, Dorame A, Bellampalli SS, Chefdeville A, Kanazawa I, Pham NYN, Park KD, Weimer JM, Khanna R. Phosphorylated CRMP2 Regulates Spinal Nociceptive Neurotransmission. Mol Neurobiol 2019;56(7):5241–5255. [PubMed: 30565051]

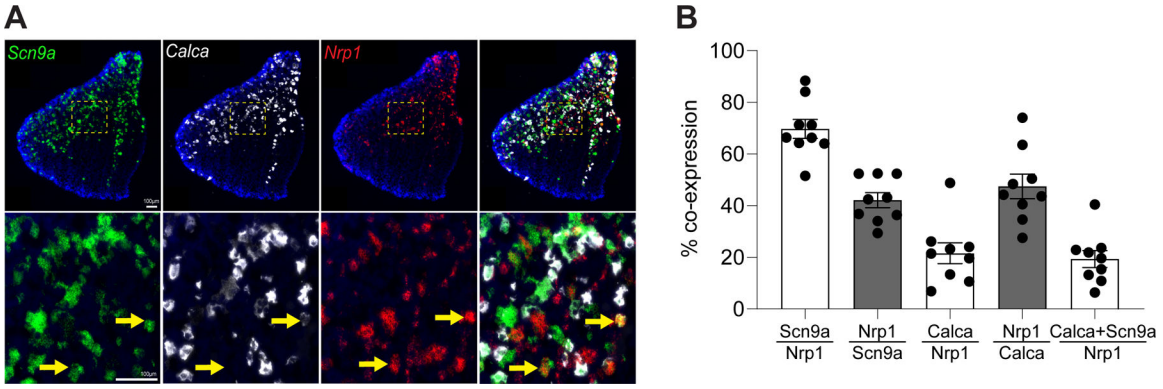

Figure 1. Nrp1 is expressed in putative nociceptors in the rat dorsal root ganglion.

A) Representative images of triple label fluorescence in situ hybridization for Scn9a, Calca, and Nrp1 in the lumbar dorsal root ganglion of naïve adult rats. In addition, nuclei are labeled with the nuclear labeling dye 49,6-diamidino-2-phenylindole (DAPI). Yellow arrows indicate co-localization. B) Nrp1 extensively co-localizes with Scn9a (Scn9a/Nrp1: 69.73 ± 3.68%; Nrp1/Scn9a: 42.15 ± 2.91%), Calca (Calca/Nrp1: 21.56 ± 4.05%; Nrp1/Calca: 47.44 ± 4.73%), and Calca + Scn9a (Calca + Scn9a/Nrp1: 19.36 ± 3.29%). n=9 rats. Individual data points represent the mean of 3–8 sections from two DRGs per individual rat. Scale bars: 100 μm. Error bars indicate mean ± SEM.

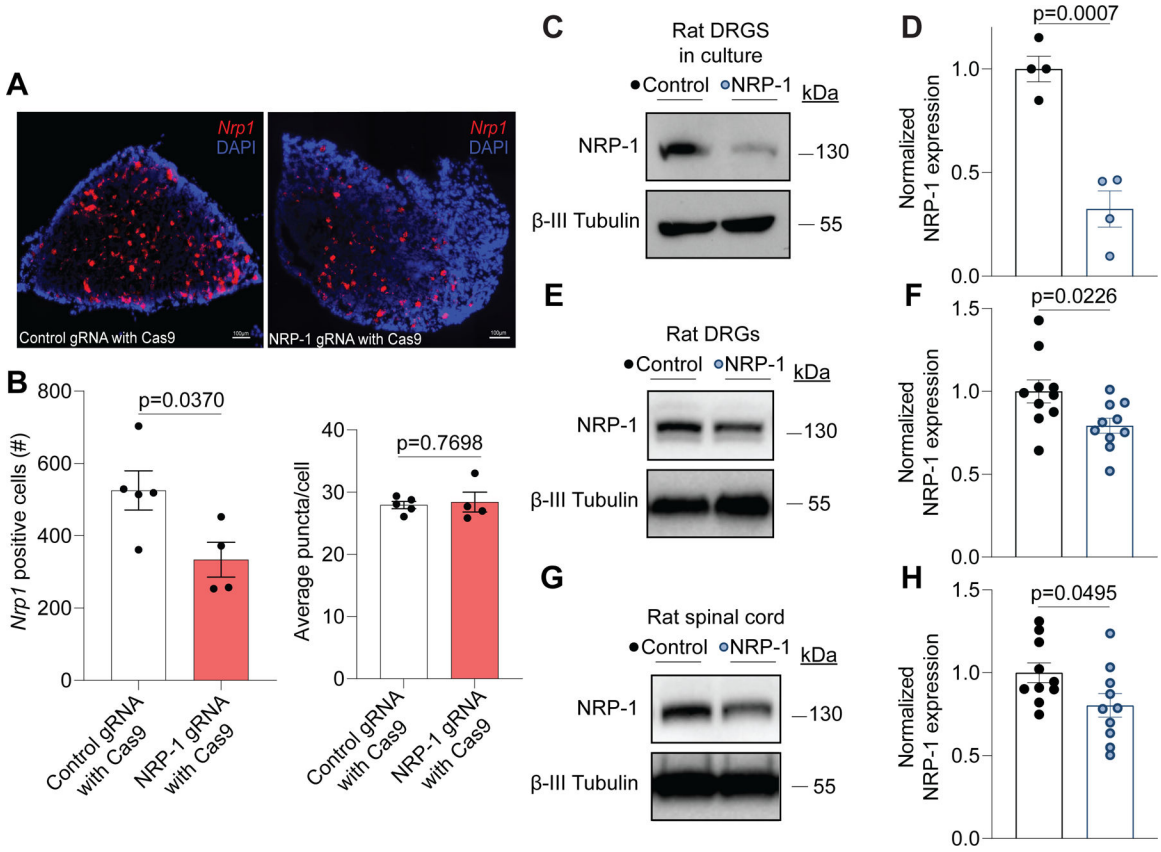

Figure 2. Validation of NRP-1 knockdown in rat dorsal root ganglia neurons through CRISPR/Cas9 editing.

A) Representative images of *Nrp1* expression in rat DRGs 7 days after intrathecal administration of lentivirus particles (~ $1x10^6$ IFU/mL) containing pL-CRISPR-EFS-GFP (Control gRNA with Cas9) or pL-CRISPR-EFS-GFP-rNRP-1 (NRP-1 gRNA with Cas9). Scale bars: 100 μm. B) Bar graphs with scatter plots showing that intrathecal NRP-1 gRNA with Cas9-mediated knockdown reduces the number of DRG neurons that express *Nrp1* without changing the average puncta per cell. n= 4–5 rats. C) Representative immunoblots showing the expression of NRP-1 in DRGs of rats transfected with either pL-CRISPR-EFS-GFP (Control) or pL-CRISPR-EFS-GFP-rNRP-1 (NRP-1) plasmids. βIII-Tubulin is used as a loading control. D) Bar graph with scatter plots showing the quantification of (C), n= 4 samples. Representative immunoblots showing the expression of NRP-1 in DRGs (E) and spinal cord (G) tissue of rats 7 days after intrathecal administration of lentivirus particles (~ $1x10^6$ IFU/mL) containing pL-CRISPR-EFS-GFP (Control) or pL-CRISPR-EFS-GFP-rNRP-1 (NRP-1). βIII-Tubulin is used as a loading control. Bar graph with scatter plots showing the quantification of DRGs (F) and spinal cord (H) of n= 10 samples. *p* values as indicated; Unpaired t test; Error bars indicate mean ± SEM. For full statistical analyses, see Table S1.

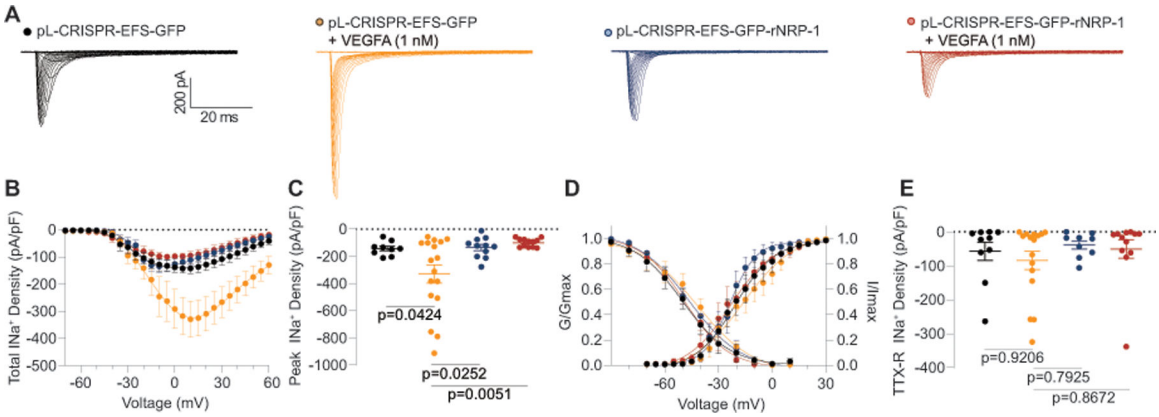

Figure 3. VEGFA-induced increase in sodium currents is attenuated by NRP-1 knockdown.

A) Representative sodium current traces recorded from rat DRG neurons 48 hours after transfection with pL-CRISPR-EFS-GFP (Control CRISPR) or pL-CRISPR-EFS-GFP-rNRP-1 (NRP-1 CRISPR) plasmids incubated with and without rat VEGFA (1 nM, 30 min). B) Double Boltzmann fits for current density–voltage curves of each of the above conditions showing that VEGFA enhances sodium currents, and that this effect can be attenuated when NRP-1 is absent. C) Summary of bar graph showing peak sodium current densities for the indicated conditions showing that NRP-1 knockdown blocks VEGFA-induced increase in peak current density. D) Boltzmann fits for voltage-dependent activation and inactivation kinetics as shown. Half-maximal activation potential of activation and inactivation ($V_{1/2}$) and slope values (k) for activation and inactivation are reported in Table S2. E) Summary of bar graph showing peak TTX-resistant sodium current densities for the indicated conditions showing VEGFA treatment or NRP-1 knockdown have no effect in these currents. p values as indicated; One-way ANOVA followed by Tukey's multiple comparisons test; N=9–17 cells; Error bars indicate mean ± SEM. For full statistical analyses, see Table S1.

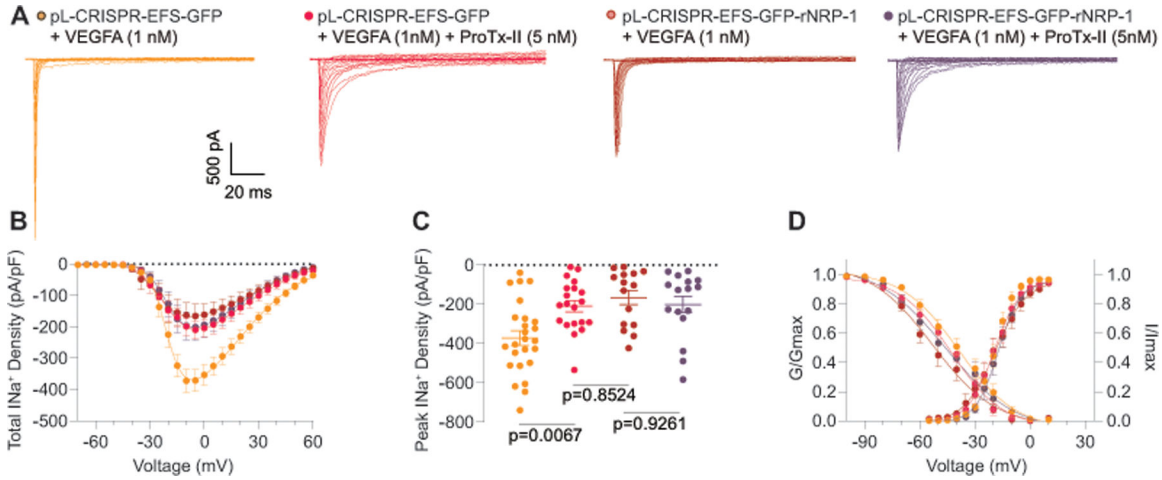

Figure 4. VEGFA-mediated increase in sodium current density is due to NaV1.7 channels.

(A) Representative families of sodium current traces obtained from DRG neurons following treatment with the indicated compound or protein 48 hours after transfection with pL-CRISPR-EFS-GFP (Control CRISPR) or pL-CRISPR-EFS-GFP-rNRP-1 (NRP-1 CRISPR). B) Double Boltzmann fits of current density–voltage curves for each of the conditions showing that VEGFA enhances sodium currents, and that this enhancement can be blocked by co-application of PrTx-II (5 nM), a selective NaV1.7 blocker. When NRP-1 is not present, PrTx-II does not further decrease sodium currents. C) Summary of bar graph showing peak sodium current densities for the indicated conditions showing that ProTx-II blocks VEGFA-induced increase in peak current density. D) Boltzmann fits for voltage-dependent activation and inactivation as shown. Half-maximal activation potential of activation and inactivation ($V_{1/2}$) and slope factor values (k) for activation and inactivation are presented in Table S2. p values as indicated; One-way ANOVA followed by Tukey's multiple comparisons test; N=15–25 cells; Error bars indicate mean ± SEM. For full statistical analyses, see Table S1.

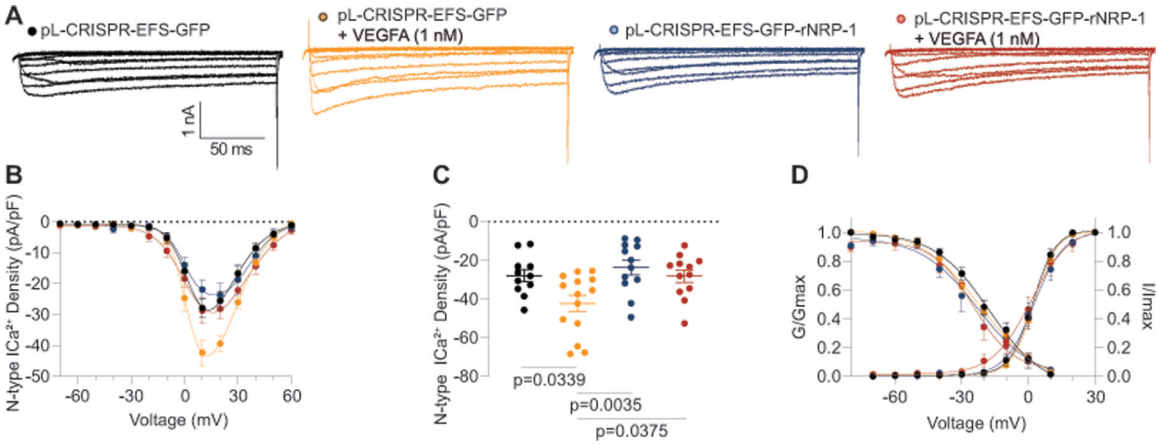

Figure 5. CRISPR-mediated knockdown of NRP-1 in sensory neurons prevents VEGFA-mediated increase in CaV2.2 (N-type) currents.

A) Representative families of calcium currents recorded from rat DRG neurons 48 hours after transfection with pL-CRISPR-EFS-GFP (Control CRISPR) or pL-CRISPR-EFS-GFP-rNRP-1 (NRP-1 CRISPR) plasmids incubated in the presence and absence of rat VEGFA (1 nM). B) Double Boltzmann fits of current density–voltage curves for each of the conditions demonstrating that enhancement of N-type calcium currents by VEGFA is attenuated when NRP-1 is not present. C) Summary of bar graph showing peak N-type current densities for the indicated conditions illustrating that knocking-down NRP1–4 blocks the VEGFA-induced increase in peak current density. D) Boltzmann fits for voltage-dependent activation and inactivation as shown. Half-maximal activation potential of activation and inactivation ($V_{1/2}$) and slope factor values (k) for activation and inactivation are presented in Table S2. p values as indicated; One-way ANOVA followed by Tukey's multiple comparisons test; N=11–14 cells; Error bars indicate mean ± SEM. For full statistical analyses, see Table S1.

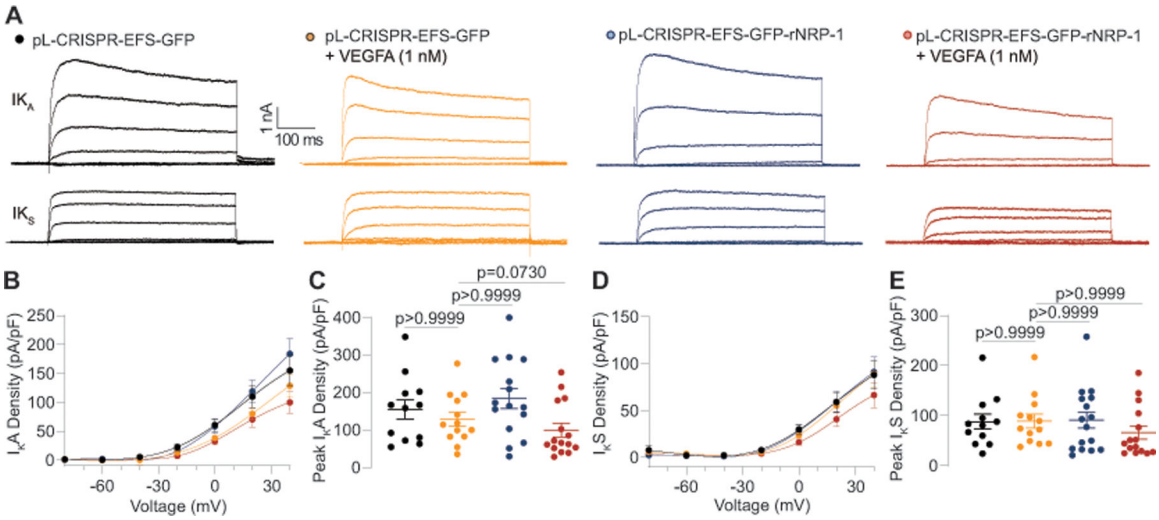

Figure 6. NRP-1 knockdown does not affect voltage-gated potassium channels expressed in DRG neurons.

A) Representative IK_A and IK_S potassium current traces recorded from DRGs 48 hours after transfection with pL-CRISPR-EFS-GFP (Control CRISPR) or pL-CRISPR-EFS-GFP-rNRP-1 (NRP-1 CRISPR) plasmids with and without incubation with rat VEGFA (1 nM). B) Double Boltzmann fits for current density-voltage curves of IK_A currents. C) Summary of peak IK_A current densities (pA/pF). Addition of VEGFA nor knockdown of NRP-1 affect IK_A currents. D) Double Boltzmann fits for current density-voltage curves of IK_S currents. E) Summary of peak IK_S current densities (pA/pF). Adding VEGFA or eliminating NRP-1 did not affect IK_A currents. *p* values as indicated; Kruskal-Wallis test followed by Dunn's test for multiple comparisons; N=12–16 cells; Error bars indicate mean ± SEM. For full statistical analyses, see Table S1.

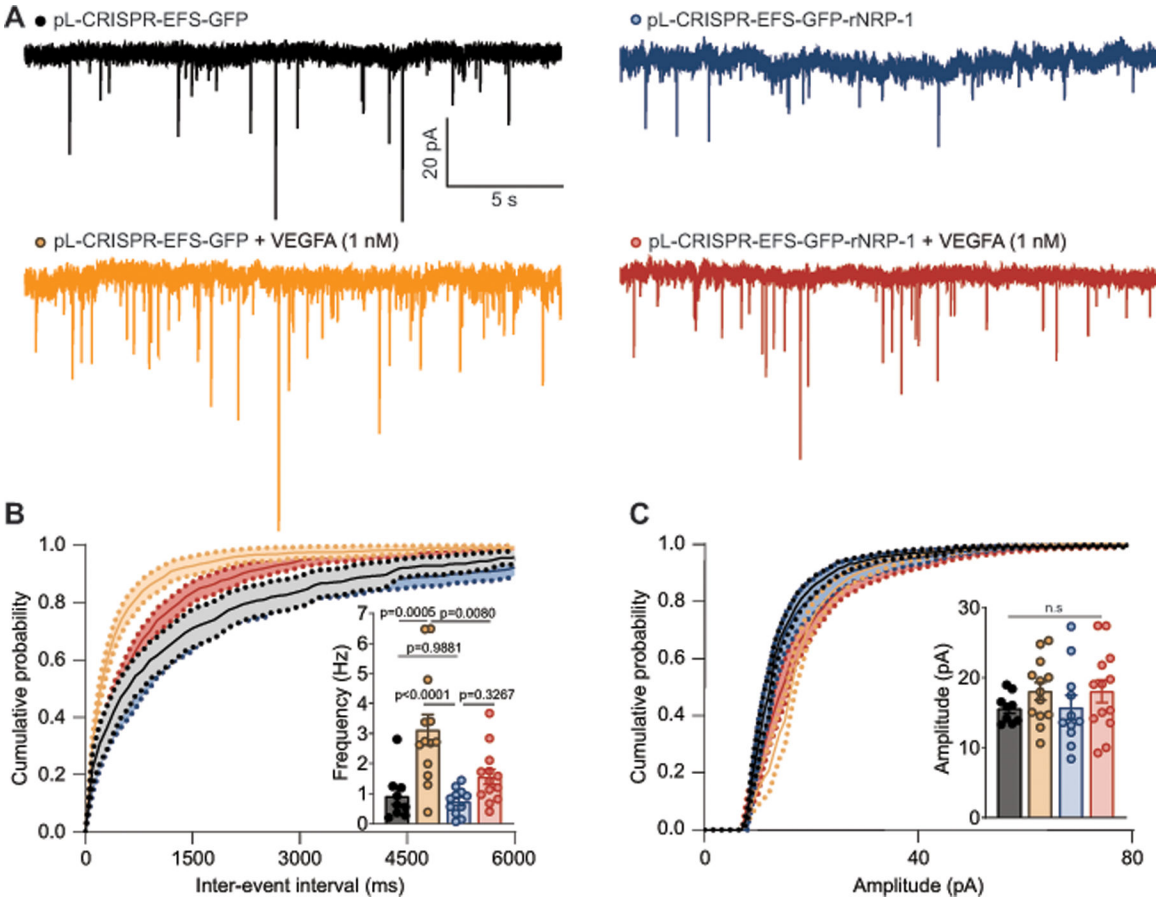

Figure 7. CRISPR-mediated knockdown of NRP-1 decreases VEGFA-mediated increase in frequency of spontaneous excitatory postsynaptic currents (sEPSCs) in the substantia gelatinosa region of the lumbar dorsal horn.

A) Representative traces of sEPSC recordings from substantia gelatinosa (SG) neurons transfected with either pL-CRISPR-EFS-GFP (Control CRISPR) or pL-CRISPR-EFS-GFP-rNRP-1 (NRP-1 CRISPR) plasmids. B) Cumulative distribution of sEPSC inter-event intervals recorded from SG neurons. Inset: Bar graph with scatter plot showing sEPSC frequency. C) Cumulative distribution of sEPSC amplitudes intervals recorded from SG neurons. Inset: Bar graph with scatter plot showing sEPSC amplitude. Addition of VEGFA increased the frequency, but not the amplitude, of sEPSC in the SDH. Selective knockdown of NRP-1 blocked the effect of VEGFA. *p* values as indicated; One-way ANOVA followed by Tukey's multiple comparisons test; N=9–13 cells; Error bars indicate mean ± SEM. For full statistical analyses, see Table S1.

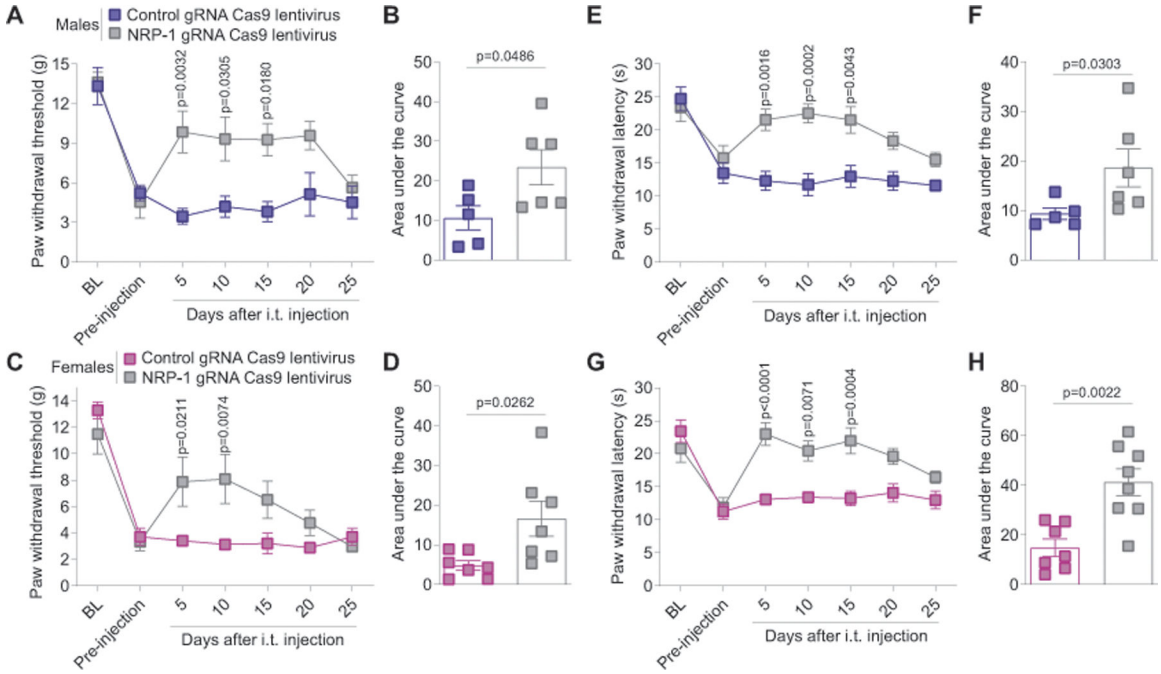

Figure 8. *In vivo* NRP-1 knockdown reverses mechanical allodynia and thermal hyperalgesia following spinal nerve ligation in male and female rats.

L5/L6 spinal nerve ligation (SNL) was performed in male and female rats to induce chronic neuropathic pain. Fourteen days post-surgery, animals were administered with lentiviral particles (~ $1x10^6$ IFU/mL) containing pL-CRISPR-EFS-GFP (Control gRNA Cas9 lentivirus) or pL-CRISPR-EFS-GFP-rNRP-1 (NRP-1 gRNA Cas9 lentivirus) through intrathecal (i.t.) injections. Paw withdrawal thresholds (A—male and C—female) and latencies (E—male and G—female) were measured before spinal nerve ligation (baseline; BL), 14 days after surgery (pre-injection or day 0), and 5, 10, 15, 20 and 25 days after intrathecal injection of lentiviral particles. Panels B, F, D, and H are the area under the curve for 0 (pre-injection) to 25 days after lentiviral administration. Knocking-down NRP-1 had an antinociceptive effect in both male and female rats. *p* values as indicated; Paw withdrawal thresholds and latencies were analyzed by Two-way ANOVA followed by Bonferroni's multiple comparisons test; Area under the curve was analyzed by Unpaired t-test; N=5–8 animals; Error bars indicate mean ± SEM. For full statistical analyses, see Table S1.